

Modeling of frequency-domain elastic-wave equation with an average-derivative optimal method

Jing-Bo Chen¹ and Jian Cao¹

ABSTRACT

Based on an average-derivative method, we developed a new nine-point numerical scheme for a frequency-domain elastic-wave equation. Compared with the classic nine-point scheme, this scheme reduces the required number of grid points per wavelength for equal and unequal directional spacings. The reduction in the number of grid points increases as the Poisson's ratio becomes larger. In particular, as the Poisson's ratio reaches 0.5, the numerical S-wave phase velocity of this new scheme becomes zero, whereas the classical scheme produces spurious numerical S-wave phase velocity. Numerical examples demonstrate that this new scheme produces more accurate results than the classical scheme at approximately the same computational cost.

INTRODUCTION

Frequency-domain numerical modeling of seismic-wave equations was pioneered by [Lysmer and Drake \(1972\)](#) to describe the wave propagation in the earth. In analyzing the accuracy of finite-difference and finite-element modeling of the scalar- and elastic-wave equations, [Marfurt \(1984\)](#) further examines frequency-domain numerical modeling. One of Marfurt's important research results is that frequency-domain finite-element solutions using a weighted average of consistent and lumped masses lead to accurate results. [Pratt and Worthington \(1990\)](#) present in detail the implementation of the classical five-point scheme for frequency-domain 2D acoustic-wave equation and apply it to multisource crosshole tomography. Based on the spatial approximations in [Kelly et al. \(1976\)](#), [Pratt \(1990\)](#) develops a classic nine-point scheme for frequency-domain 2D elastic-wave equation. Because of its small bandwidth in the resulting impedance matrix, this scheme is very efficient. To reduce numerical

dispersion, however, this classical scheme requires a large number of grid points per wavelength.

Based on a rotated coordinates system and averaging mass acceleration terms, [Jo et al. \(1996\)](#) develop an optimal nine-point scheme for 2D scalar-wave equation. The optimization coefficients are obtained by minimizing the phase velocity errors. This scheme reduces the number of grid points per wavelength from 13 to 4 in comparison with the classical five-point scheme. For frequency-domain numerical modeling, [Jo et al.'s \(1996\)](#) method is an important optimization approach. This approach is then generalized to a variable-density case ([Hustedt et al., 2004](#)) and a 3D case ([Operto et al., 2007](#)). Schemes involving more grid points have also been developed ([Shin and Sohn, 1998](#); [Min et al., 2000](#); [Gu et al., 2013](#)). These schemes have higher accuracy but lower efficiency.

For frequency-domain elastic-wave modeling, [Štekl and Pratt \(1998\)](#) propose an optimal nine-point scheme for frequency-domain 2D elastic-wave equation. The construction of the optimal scheme incorporates [Jo et al.'s \(1996\)](#) method and staggered-grid technique. This optimal nine-point scheme is particularly desirable because it not only reduces the number of grid points per wavelength but also remains approximately the same in terms of computational cost. However, this optimal scheme suffers from two limitations: (1) It requires equal directional grid intervals and (2) when generalized to the 3D case, it becomes very complicated and requires a lot of transformations ([Operto et al., 2007](#)).

To address these two limitations, we will develop an average-derivative optimal method for the frequency-domain elastic-wave equation. This method is a generalization of the corresponding approach for the acoustic-wave equation ([Chen, 2012, 2014](#)) and results in an average-derivative optimal nine-point scheme for frequency-domain 2D elastic-wave equation. This new average-derivative optimal nine-point scheme not only preserves the advantages of the optimal scheme proposed by [Štekl and Pratt \(1998\)](#) but also accommodates arbitrary directional grid intervals. In addition, this average-derivative optimal nine-point scheme can be easily

Manuscript received by the Editor 21 January 2016; revised manuscript received 15 June 2016; published online 23 September 2016.

¹Institute of Geology and Geophysics, Key Laboratory of Petroleum Resources Research, Chinese Academy of Sciences, Beijing, China and University of Chinese Academy of Sciences, Beijing, China. E-mail: chenjb@mail.iggcas.ac.cn; chris40474047@163.com.

© 2016 Society of Exploration Geophysicists. All rights reserved.

generalized to a 27-point scheme for the frequency-domain 3D elastic-wave equation.

In the next section, we will present the average-derivative numerical method for the frequency-domain elastic-wave equation. This is followed by a numerical dispersion analysis. Then, we present numerical examples to demonstrate the theoretical analysis.

AN AVERAGE-DERIVATIVE METHOD

We consider the 2D elastic-wave equation in the frequency domain:

$$\frac{\partial}{\partial x} \left(\eta \frac{\partial u}{\partial x} \right) + \frac{\partial}{\partial z} \left(\mu \frac{\partial u}{\partial z} \right) + \frac{\partial}{\partial x} \left(\lambda \frac{\partial w}{\partial z} \right) + \frac{\partial}{\partial z} \left(\mu \frac{\partial w}{\partial x} \right) + \rho \omega^2 u = 0, \tag{1}$$

$$\frac{\partial}{\partial x} \left(\mu \frac{\partial w}{\partial x} \right) + \frac{\partial}{\partial z} \left(\eta \frac{\partial w}{\partial z} \right) + \frac{\partial}{\partial x} \left(\mu \frac{\partial u}{\partial z} \right) + \frac{\partial}{\partial z} \left(\lambda \frac{\partial u}{\partial x} \right) + \rho \omega^2 w = 0, \tag{2}$$

where u and w represent the horizontal and vertical displacement components, respectively, ρ is the density, ω is the circular frequency, λ and μ are the Lamé parameters, and $\eta = \lambda + 2\mu$.

We will now discretize equations 1 and 2. Set $u_{m,n} \approx u(m\Delta x, n\Delta z)$ and $w_{m,n} \approx w(m\Delta x, n\Delta z)$, where Δx and Δz are the grid intervals in the x - and z -directions, respectively. First, we deal with equation 1 and it includes five terms. For the first two terms, we discretize them with an average-derivative method (Chen, 2012):

$$\frac{\partial}{\partial x} \left(\eta \frac{\partial u}{\partial x} \right) \approx \frac{1}{\Delta x^2} \times \left[\eta_{m+\frac{1}{2},n} \bar{u}_{m+1,n} - (\eta_{m+\frac{1}{2},n} + \eta_{m-\frac{1}{2},n}) \bar{u}_{m,n} + \eta_{m-\frac{1}{2},n} \bar{u}_{m-1,n} \right], \tag{3}$$

$$\frac{\partial}{\partial z} \left(\mu \frac{\partial u}{\partial z} \right) \approx \frac{1}{\Delta z^2} \times \left[\mu_{m,n+\frac{1}{2}} \tilde{u}_{m,n+1} - (\mu_{m,n+\frac{1}{2}} + \mu_{m,n-\frac{1}{2}}) \tilde{u}_{m,n} + \mu_{m,n-\frac{1}{2}} \tilde{u}_{m,n-1} \right], \tag{4}$$

where

$$\begin{aligned} \eta_{m+\frac{1}{2},n} &= \frac{1}{2}(\eta_{m,n} + \eta_{m+1,n}), & \eta_{m-\frac{1}{2},n} &= \frac{1}{2}(\eta_{m-1,n} + \eta_{m,n}), \\ \eta_{m,n+\frac{1}{2}} &= \frac{1}{2}(\eta_{m,n} + \eta_{m,n+1}), & \eta_{m,n-\frac{1}{2}} &= \frac{1}{2}(\eta_{m,n-1} + \eta_{m,n}), \\ \mu_{m+\frac{1}{2},n} &= \frac{1}{2}(\mu_{m,n} + \mu_{m+1,n}), & \mu_{m-\frac{1}{2},n} &= \frac{1}{2}(\mu_{m-1,n} + \mu_{m,n}), \\ \mu_{m,n+\frac{1}{2}} &= \frac{1}{2}(\mu_{m,n} + \mu_{m,n+1}), & \mu_{m,n-\frac{1}{2}} &= \frac{1}{2}(\mu_{m,n-1} + \mu_{m,n}), \end{aligned} \tag{5}$$

and

$$\begin{aligned} \bar{u}_{m+j,n} &= \frac{1-\gamma_1}{2} u_{m+j,n+1} + \gamma_1 u_{m+j,n} + \frac{1-\gamma_1}{2} u_{m+j,n-1}, & j &= -1, 0, 1, \\ \tilde{u}_{m,n+j} &= \frac{1-\gamma_2}{2} u_{m+1,n+j} + \gamma_2 u_{m,n+j} + \frac{1-\gamma_2}{2} u_{m-1,n+j}, & j &= -1, 0, 1. \end{aligned} \tag{6}$$

Here, γ_1 and γ_2 are the weighted coefficients.

For the third and fourth terms in equation 1, we use the centered differences:

$$\begin{aligned} \frac{\partial}{\partial x} \left(\lambda \frac{\partial w}{\partial z} \right) &\approx \frac{1}{4\Delta x \Delta z} [\lambda_{m+1,n} (w_{m+1,n+1} - w_{m+1,n-1}) \\ &- \lambda_{m-1,n} (w_{m-1,n+1} - w_{m-1,n-1})], \end{aligned} \tag{7}$$

$$\begin{aligned} \frac{\partial}{\partial z} \left(\mu \frac{\partial w}{\partial x} \right) &\approx \frac{1}{4\Delta x \Delta z} [\mu_{m,n+1} (w_{m+1,n+1} - w_{m-1,n+1}) \\ &- \mu_{m,n-1} (w_{m+1,n-1} - w_{m-1,n-1})]. \end{aligned} \tag{8}$$

For the fifth term in equation 1, we use the weighted average:

$$\rho \omega^2 u \approx \rho_{m,n} \omega^2 [c u_{m,n} + d(u_{m+1,n} + u_{m-1,n} + u_{m,n+1} + u_{m,n-1}) + e(u_{m+1,n+1} + u_{m-1,n+1} + u_{m+1,n-1} + u_{m-1,n-1})], \tag{9}$$

where c and d are the weighted coefficients and $e = (1 - c - 4d)/4$.

Substituting equations 3–9 into equation 1, and performing the same discretizations for equation 2, we obtain an average-derivative nine-point scheme for equations 1 and 2:

$$\begin{aligned} &\frac{1}{\Delta x^2} \left[\eta_{m+\frac{1}{2},n} \bar{u}_{m+1,n} - (\eta_{m+\frac{1}{2},n} + \eta_{m-\frac{1}{2},n}) \bar{u}_{m,n} + \eta_{m-\frac{1}{2},n} \bar{u}_{m-1,n} \right] \\ &+ \frac{1}{\Delta z^2} \left[\mu_{m,n+\frac{1}{2}} \tilde{u}_{m,n+1} - (\mu_{m,n+\frac{1}{2}} + \mu_{m,n-\frac{1}{2}}) \tilde{u}_{m,n} + \mu_{m,n-\frac{1}{2}} \tilde{u}_{m,n-1} \right] \\ &+ \frac{1}{4\Delta x \Delta z} [\lambda_{m+1,n} (w_{m+1,n+1} - w_{m+1,n-1}) \\ &- \lambda_{m-1,n} (w_{m-1,n+1} - w_{m-1,n-1})] \\ &+ \frac{1}{4\Delta x \Delta z} [\mu_{m,n+1} (w_{m+1,n+1} - w_{m-1,n+1}) \\ &- \mu_{m,n-1} (w_{m+1,n-1} - w_{m-1,n-1})] \\ &+ \rho_{m,n} \omega^2 [c u_{m,n} + d(u_{m+1,n} + u_{m-1,n} + u_{m,n+1} + u_{m,n-1}) \\ &+ e(u_{m+1,n+1} + u_{m-1,n+1} + u_{m+1,n-1} + u_{m-1,n-1})] = 0, \end{aligned} \tag{10}$$

$$\begin{aligned} & \frac{1}{\Delta x^2} \left[\mu_{m+\frac{1}{2},n} \bar{w}_{m+1,n} - \left(\mu_{m+\frac{1}{2},n} + \mu_{m-\frac{1}{2},n} \right) \bar{w}_{m,n} + \mu_{m-\frac{1}{2},n} \bar{w}_{m-1,n} \right] \\ & + \frac{1}{\Delta z^2} \left[\eta_{m,n+\frac{1}{2}} \tilde{w}_{m,n+1} - \left(\eta_{m,n+\frac{1}{2}} + \eta_{m,n-\frac{1}{2}} \right) \tilde{w}_{m,n} + \eta_{m,n-\frac{1}{2}} \tilde{w}_{m,n-1} \right] \\ & + \frac{1}{4\Delta x\Delta z} \left[\mu_{m+1,n} (u_{m+1,n+1} - u_{m+1,n-1}) \right. \\ & \quad \left. - \mu_{m-1,n} (u_{m-1,n+1} - u_{m-1,n-1}) \right] \\ & + \frac{1}{4\Delta x\Delta z} \left[\lambda_{m,n+1} (u_{m+1,n+1} - u_{m-1,n+1}) \right. \\ & \quad \left. - \lambda_{m,n-1} (u_{m+1,n-1} - u_{m-1,n-1}) \right] \\ & + \rho_{m,n} \omega^2 [c w_{m,n} + d(w_{m+1,n} + w_{m-1,n} + w_{m,n+1} + w_{m,n-1}) \\ & \quad + e(w_{m+1,n+1} + w_{m-1,n+1} + w_{m+1,n-1} + w_{m-1,n-1})] = 0. \end{aligned} \quad (11)$$

Figure 1 shows the stencil of the average-derivative nine-point scheme 10 and 11. If we take $\gamma_1 = \gamma_2 = c = 1$ and $d = 0$, the average-derivative nine-point scheme 10 and 11 reduces to the classical nine-point scheme (Pratt, 1990):

$$\begin{aligned} & \frac{1}{\Delta x^2} \left[\eta_{m+\frac{1}{2},n} u_{m+1,n} - \left(\eta_{m+\frac{1}{2},n} + \eta_{m-\frac{1}{2},n} \right) u_{m,n} + \eta_{m-\frac{1}{2},n} u_{m-1,n} \right] \\ & + \frac{1}{\Delta z^2} \left[\mu_{m,n+\frac{1}{2}} u_{m,n+1} - \left(\mu_{m,n+\frac{1}{2}} + \mu_{m,n-\frac{1}{2}} \right) u_{m,n} + \mu_{m,n-\frac{1}{2}} u_{m,n-1} \right] \\ & + \frac{1}{4\Delta x\Delta z} \left[\lambda_{m+1,n} (w_{m+1,n+1} - w_{m+1,n-1}) \right. \\ & \quad \left. - \lambda_{m-1,n} (w_{m-1,n+1} - w_{m-1,n-1}) \right] \\ & + \frac{1}{4\Delta x\Delta z} \left[\mu_{m,n+1} (w_{m+1,n+1} - w_{m-1,n+1}) \right. \\ & \quad \left. - \mu_{m,n-1} (w_{m+1,n-1} - w_{m-1,n-1}) \right] \\ & + \rho_{m,n} \omega^2 u_{m,n} = 0, \end{aligned} \quad (12)$$

$$\begin{aligned} & \frac{1}{\Delta x^2} \left[\mu_{m+\frac{1}{2},n} w_{m+1,n} - \left(\mu_{m+\frac{1}{2},n} + \mu_{m-\frac{1}{2},n} \right) w_{m,n} + \mu_{m-\frac{1}{2},n} w_{m-1,n} \right] \\ & + \frac{1}{\Delta z^2} \left[\eta_{m,n+\frac{1}{2}} w_{m,n+1} - \left(\eta_{m,n+\frac{1}{2}} + \eta_{m,n-\frac{1}{2}} \right) w_{m,n} + \eta_{m,n-\frac{1}{2}} w_{m,n-1} \right] \\ & + \frac{1}{4\Delta x\Delta z} \left[\mu_{m+1,n} (u_{m+1,n+1} - u_{m+1,n-1}) \right. \\ & \quad \left. - \mu_{m-1,n} (u_{m-1,n+1} - u_{m-1,n-1}) \right] \\ & + \frac{1}{4\Delta x\Delta z} \left[\lambda_{m,n+1} (u_{m+1,n+1} - u_{m-1,n+1}) \right. \\ & \quad \left. - \lambda_{m,n-1} (u_{m+1,n-1} - u_{m-1,n-1}) \right] \\ & + \rho_{m,n} \omega^2 w_{m,n} = 0. \end{aligned} \quad (13)$$

The average-derivative nine-point scheme 10 and 11 can be easily generalized to an average-derivative 27-point scheme for the 3D frequency-domain elastic-wave equation (Appendix A).

NUMERICAL DISPERSION ANALYSIS

We will now perform numerical dispersion analysis for the average-derivative nine-point scheme 10 and 11. Set

$$\begin{bmatrix} u \\ v \end{bmatrix} = \begin{bmatrix} u_0 \\ v_0 \end{bmatrix} e^{i(k_x x + k_z z)}, \quad (14)$$

where u_0 and v_0 are the constants that are not equal to zero simultaneously and k_x and k_z are the horizontal and vertical wavenumbers, respectively.

Substituting equation 14 into the scheme 10 and 11 and setting the determinant of the resulting matrix to be zero, we obtain the P- and S-wave dispersion relations:

$$\begin{aligned} \omega^2 &= \frac{1}{2\mathcal{E}\Delta x^2} \left[(\alpha^2 + \beta^2)(\mathcal{E}_{xx} + \mathcal{E}_{zz}) \right. \\ & \quad \left. + (\alpha^2 - \beta^2) \sqrt{(\mathcal{E}_{xx} - \mathcal{E}_{zz})^2 + 4\mathcal{E}_{xz}^2} \right], \end{aligned} \quad (15)$$

$$\begin{aligned} \omega^2 &= \frac{1}{2\mathcal{E}\Delta x^2} \left[(\alpha^2 + \beta^2)(\mathcal{E}_{xx} + \mathcal{E}_{zz}) \right. \\ & \quad \left. - (\alpha^2 - \beta^2) \sqrt{(\mathcal{E}_{xx} - \mathcal{E}_{zz})^2 + 4\mathcal{E}_{xz}^2} \right], \end{aligned} \quad (16)$$

where α and β are the P- and S-wave velocities, respectively, and

$$\begin{aligned} \mathcal{E} &= c + 2d(\cos(k_x \Delta x) + \cos(k_z \Delta z)) \\ & \quad + 4e \cos(k_x \Delta x) \cos(k_z \Delta z), \end{aligned} \quad (17)$$

$$\mathcal{E}_{xx} = [(1 - \gamma_1) \cos(k_z \Delta z) + \gamma_1][2 - 2 \cos(k_x \Delta x)], \quad (18)$$

$$\mathcal{E}_{zz} = r^2[(1 - \gamma_2) \cos(k_x \Delta x) + \gamma_2][2 - 2 \cos(k_z \Delta z)], \quad (19)$$

$$\mathcal{E}_{xz} = r \sin(k_x \Delta x) \sin(k_z \Delta z), \quad (20)$$

where $r = \Delta x / \Delta z$. Here without loss of generality, we suppose that $\Delta x \geq \Delta z$.

Let α_{ph} and β_{ph} denote the compressional and shear phase velocities, respectively. They are defined as

$$\alpha_{ph} = \frac{\omega}{k_p}, \quad \beta_{ph} = \frac{\omega}{k_s}, \quad (21)$$

where k_p and k_s are the compressional and shear wavenumbers, respectively.

From equations 15–21, we can obtain the normalized compressional and shear phase velocities:

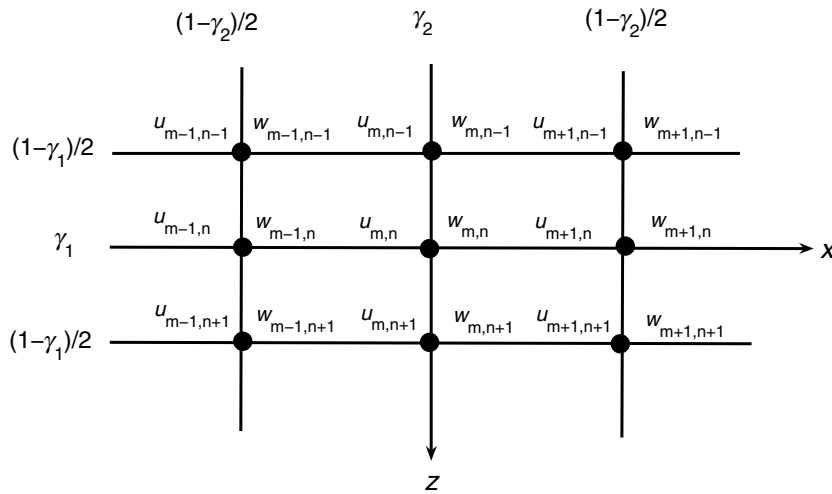


Figure 1. The stencil of the average-derivative nine-point scheme.

$$\frac{\alpha_{ph}}{\alpha} = \frac{G_s}{2\pi R} \left\{ \frac{1}{2\mathcal{E}} \left[(1+R^2)(\mathcal{E}_{xx} + \mathcal{E}_{zz}) + (1-R^2)\sqrt{(\mathcal{E}_{xx} - \mathcal{E}_{zz})^2 + 4\mathcal{E}_{xz}^2} \right] \right\}^{\frac{1}{2}}, \quad (22)$$

$$\frac{\beta_{ph}}{\beta} = \frac{G_s}{2\pi} \left\{ \frac{1}{2\mathcal{E}} \left[\left(1 + \frac{1}{R^2}\right)(\mathcal{E}_{xx} + \mathcal{E}_{zz}) + \left(1 - \frac{1}{R^2}\right)\sqrt{(\mathcal{E}_{xx} - \mathcal{E}_{zz})^2 + 4\mathcal{E}_{xz}^2} \right] \right\}^{\frac{1}{2}}, \quad (23)$$

where $R = \beta/\alpha = \sqrt{0.5 - \sigma/1 - \sigma}$, σ is the Poisson's ratio, and $G_s = 2\pi/k_s \Delta x$ is the number of grid points per shear wavelength. For the normalized P-wave phase velocity (equation 22), the expressions $k_x \Delta x$ and $k_z \Delta z$ should be replaced by

$$k_x \Delta x = \frac{2\pi R \sin \theta}{G_s}, \quad k_z \Delta z = \frac{2\pi R \cos \theta}{G_s r}, \quad (24)$$

and for the normalized S-wave phase velocity (equation 23), the expressions $k_x \Delta x$ and $k_z \Delta z$ should be replaced by

$$k_x \Delta x = \frac{2\pi \sin \theta}{G_s}, \quad k_z \Delta z = \frac{2\pi \cos \theta}{G_s r}, \quad (25)$$

where θ is the propagation angle.

The coefficients γ_1, γ_2, c , and d are determined by minimizing the phase error:

$$E(\gamma_1, \gamma_2, c, d, r, \sigma) = \iint \left\{ \left[1 - \frac{\alpha_{ph}(\tilde{k}, \theta; \gamma_1, \gamma_2, c, d, r, \sigma)}{\alpha} \right]^2 + \left[1 - \frac{\beta_{ph}(\tilde{k}, \theta; \gamma_1, \gamma_2, c, d, r, \sigma)}{\beta} \right]^2 \right\} d\tilde{k} d\theta, \quad (26)$$

where $\tilde{k} = 1/G_s$.

Table 1. The optimization coefficients for different σ with $r = \Delta x/\Delta z = 1$.

	γ_1	γ_2	c	d
$\sigma = 0.1$	0.6814	0.6814	0.6279	0.0923
$\sigma = 0.15$	0.6702	0.6702	0.6249	0.0931
$\sigma = 0.2$	0.6577	0.6577	0.6249	0.0938
$\sigma = 0.25$	0.6439	0.6439	0.6254	0.0936
$\sigma = 0.3$	0.6277	0.6277	0.6265	0.0934
$\sigma = 0.35$	0.6079	0.6079	0.6283	0.0929
$\sigma = 0.4$	0.5828	0.5828	0.6308	0.0923
$\sigma = 0.45$	0.5488	0.5488	0.6337	0.0916
$\sigma = 0.5$	0.5	0.5	0.5096	0.1226

Table 2. The optimization coefficients for different σ with $r = \Delta x/\Delta z = 1.25$.

	γ_1	γ_2	c	d
$\sigma = 0.1$	0.7334	0.6528	0.6284	0.0929
$\sigma = 0.15$	0.7179	0.6448	0.6282	0.0930
$\sigma = 0.2$	0.7009	0.6356	0.6285	0.0930
$\sigma = 0.25$	0.6875	0.6211	0.6285	0.0929
$\sigma = 0.3$	0.6646	0.6087	0.6303	0.0924
$\sigma = 0.35$	0.6535	0.6001	0.7183	0.0491
$\sigma = 0.4$	0.6053	0.5710	0.6344	0.0914
$\sigma = 0.45$	0.5619	0.5419	0.6373	0.0907
$\sigma = 0.5$	0.5	0.5	0.5145	0.1214

Table 3. The optimization coefficients for different σ with $r = \Delta x/\Delta z = 2$.

	γ_1	γ_2	c	d
$\sigma = 0.1$	0.9987	0.6118	0.6297	0.0926
$\sigma = 0.15$	0.9649	0.6062	0.6296	0.0926
$\sigma = 0.2$	0.9294	0.5994	0.6297	0.0926
$\sigma = 0.25$	0.8854	0.5923	0.6302	0.0924
$\sigma = 0.3$	0.8414	0.5830	0.6502	0.0826
$\sigma = 0.35$	0.7818	0.5699	0.6321	0.0919
$\sigma = 0.4$	0.7160	0.5546	0.6550	0.0810
$\sigma = 0.45$	0.6288	0.5331	0.7050	0.0566
$\sigma = 0.5$	0.5	0.5	0.5306	0.1173

The integration in equation 26 is usually used to simplify the optimization process (Jo et al., 1996). The ranges of \tilde{k} and θ are taken as $[0, 0.25]$ and $[0, \pi/2]$, respectively. We use a constrained nonlinear optimization program `fmincon` in MATLAB to determine the optimization coefficients. This program consists of three

kinds of algorithms: trust region reflective, active set, and interior point. The program `fmincon` is widely used in constrained nonlinear optimizations. The optimization coefficients for different σ with $r = \Delta x/\Delta z = 1$, $r = \Delta x/\Delta z = 1.25$, and $r = \Delta x/\Delta z = 2$ are listed in Tables 1, 2, and 3, respectively.

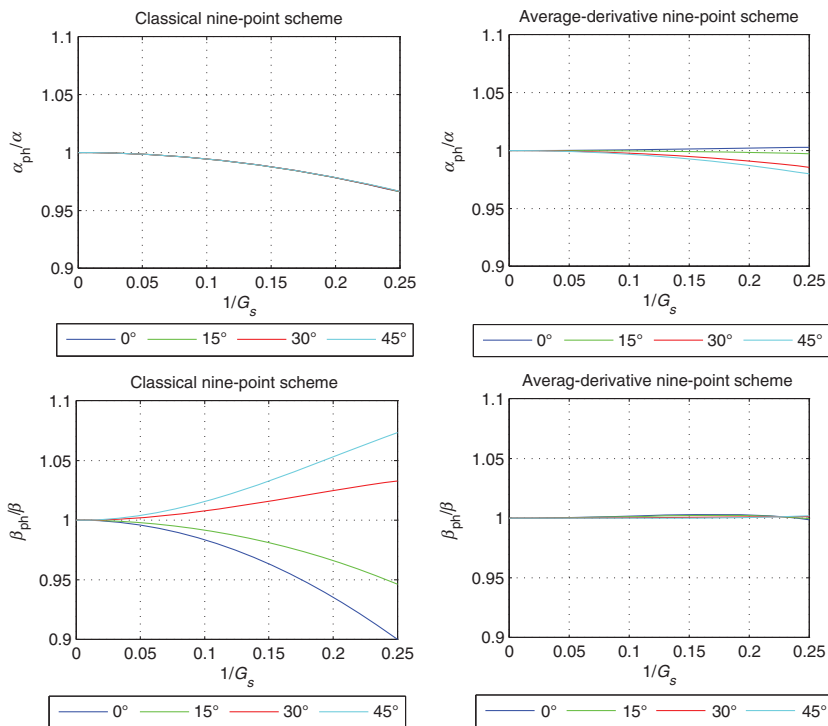


Figure 2. Normalized compressional and shear phase velocity of the classical nine-point scheme and the average-derivative optimal nine-point scheme for different propagation angles θ . Here, $\sigma = 0.25$ and $r = \Delta x/\Delta z = 1$.

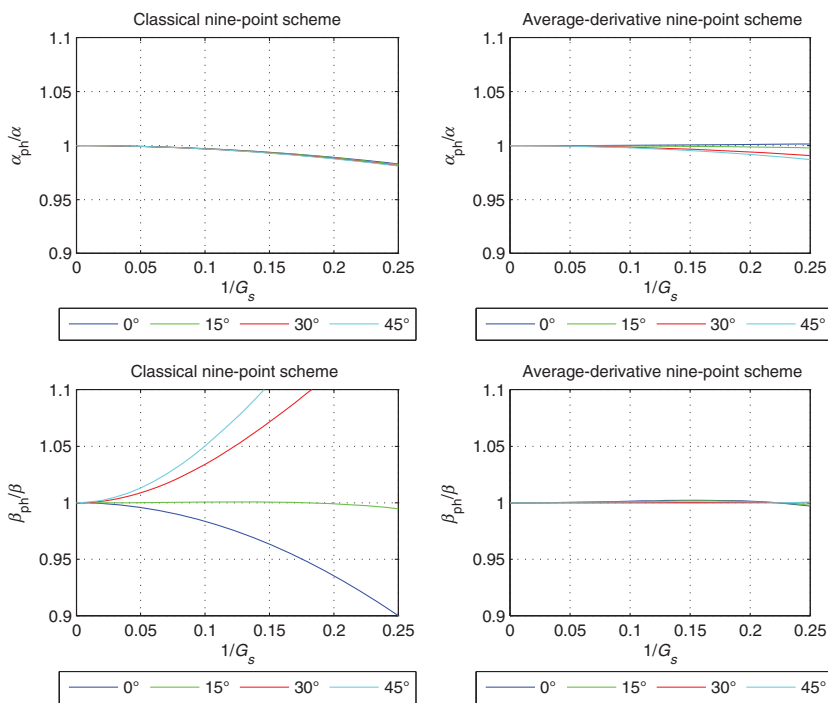


Figure 3. Normalized compressional and shear phase velocity of the classical nine-point scheme and the average-derivative optimal nine-point scheme for different propagation angles θ . Here, $\sigma = 0.4$ and $r = \Delta x/\Delta z = 1$.

Now, we make a numerical dispersion analysis and we first consider the case in which $r = \Delta x/\Delta z = 1$. Figure 2 shows normalized compressional and shear phase velocity of the classical nine-point scheme and the average-derivative optimal nine-point scheme for different propagation angles θ and for $\sigma = 0.25$. Compared with

the classical nine-point scheme, the average-derivative optimal nine-point scheme reduces the phase velocity errors, particularly for the shear phase velocity. This difference in errors reduction between compressional and shear phase velocity probably results from the optimization method. Within the phase errors of 2%, the aver-

Figure 4. Normalized compressional and shear phase velocity of the classical nine-point scheme and the average-derivative optimal nine-point scheme for different propagation angles θ . Here, $\sigma = 0.5$ and $r = \Delta x/\Delta z = 1$.

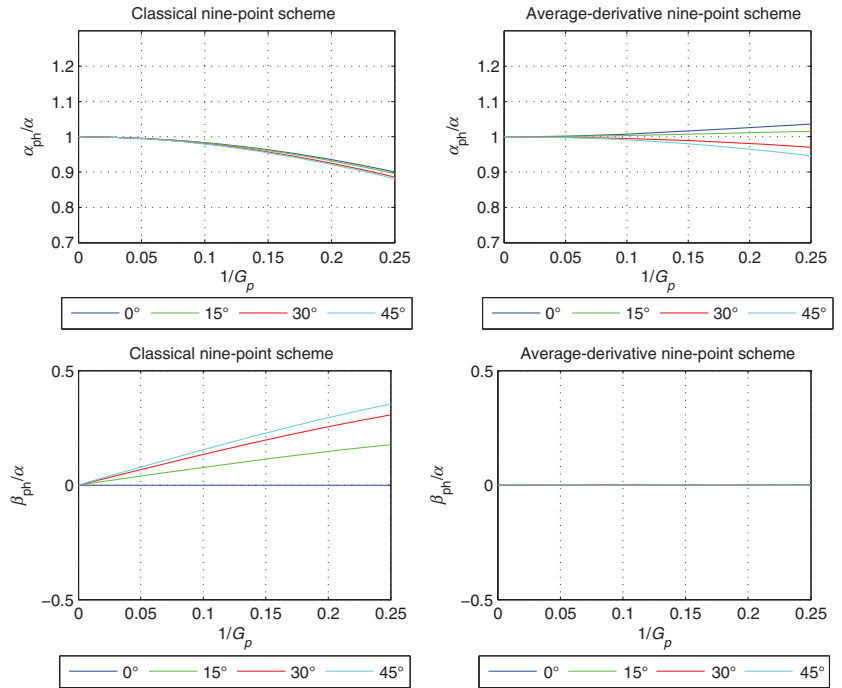
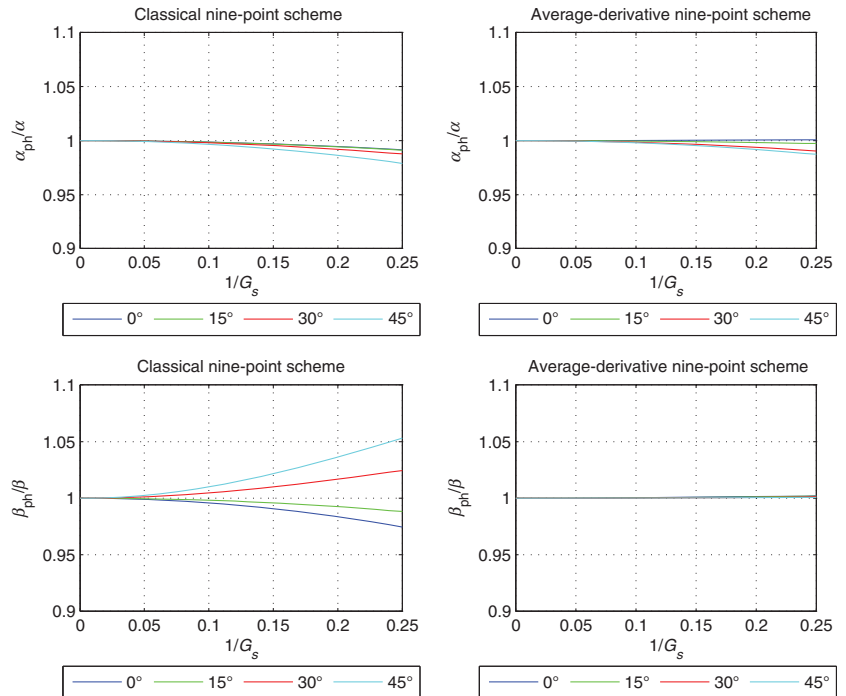


Figure 5. Normalized compressional and shear phase velocity of the classical nine-point scheme and the average-derivative optimal nine-point scheme for different propagation angles θ . Here, $\sigma = 0.25$ and $r = \Delta x/\Delta z = 2$.



age-derivative optimal nine-point scheme requires four grid points per shear wavelength, whereas for the classical nine-point scheme, it requires 10 grid points per shear wavelength. Figure 3 shows normalized compressional and shear phase velocity of the classical nine-point scheme and the average-derivative optimal nine-point scheme for different propagation angles θ and for $\sigma = 0.4$. We

can see that as σ increases, the shear phase velocity errors become larger for the classical nine-point scheme. In this case, within the phase errors of 2%, the average-derivative optimal nine-point scheme still requires four grid points per shear wavelength, whereas for the classical nine-point scheme, it requires 20 grid points per shear wavelength.

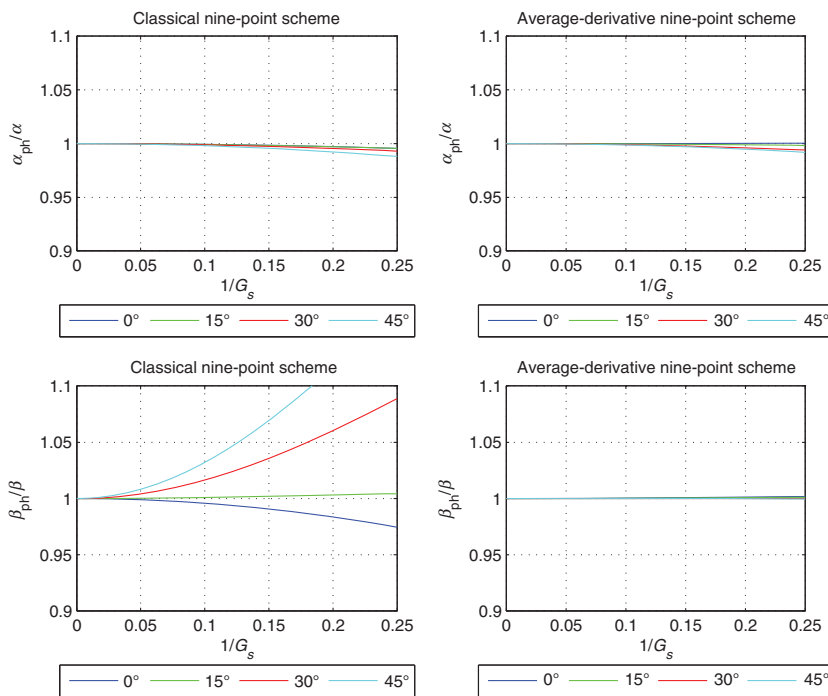


Figure 6. Normalized compressional and shear phase velocity of the classical nine-point scheme and the average-derivative optimal nine-point scheme for different propagation angles θ . Here, $\sigma = 0.4$ and $r = \Delta x/\Delta z = 2$.

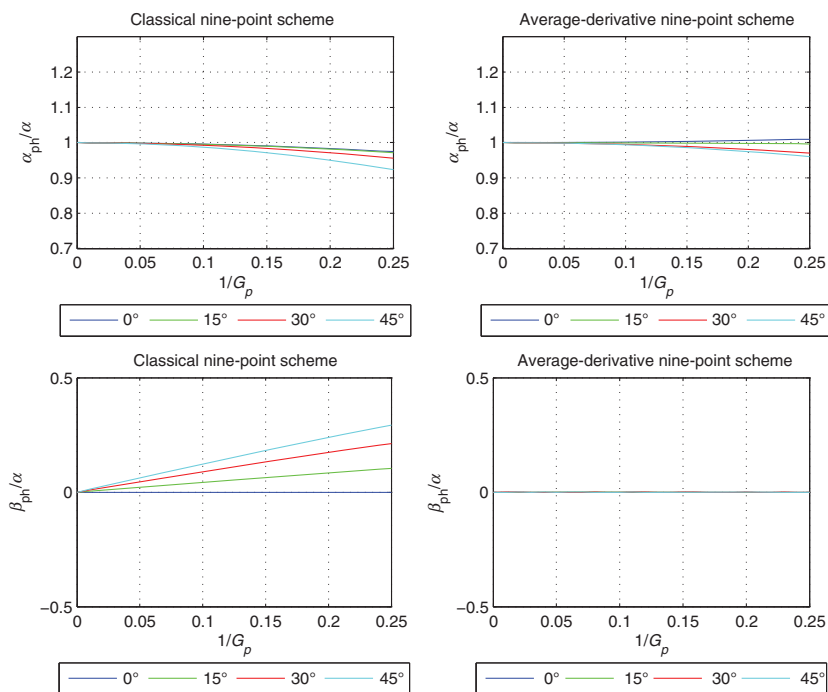


Figure 7. Normalized compressional and shear phase velocity of the classical nine-point scheme and the average-derivative optimal nine-point scheme for different propagation angles θ . Here, $\sigma = 0.5$ and $r = \Delta x/\Delta z = 2$.

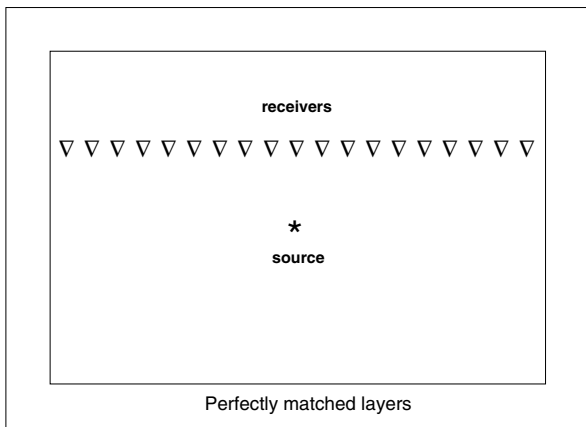
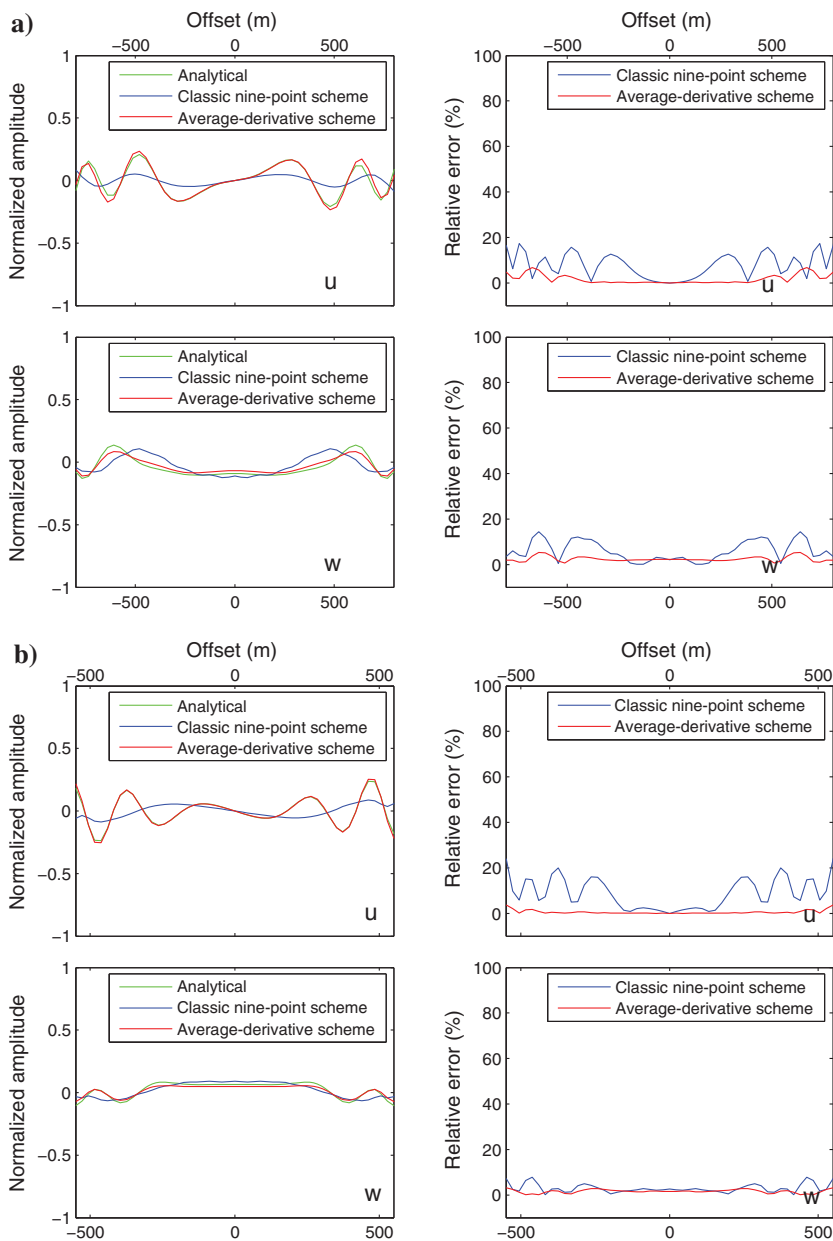


Figure 8. Schematic of the homogeneous model.

Figure 9. Frequency-domain seismograms ($\omega = 30\pi$) computed with the analytical formula (green line), the classic nine-point scheme (blue line), and the average-derivative scheme (red line). (a) $\sigma = 0.25$ and (b) $\sigma = 0.4$. Here, $\Delta x/\Delta z = 1$.



In Figure 4, we show the case in which $\sigma = 0.5$. In this case, the theoretical shear phase velocity should be zero. For the classical nine-point scheme, it produces spurious shear waves and cannot be used in this case as a result. For the average-derivative optimal nine-point scheme, the S-wave phase velocity is zero. Within the phase errors of 5%, the average-derivative optimal nine-point scheme requires four grid points per compressional wavelength. Figures 5, 6, and 7 show the situation in which $r = \Delta x/\Delta z = 2$. Because of the relatively smaller Δz , the corresponding phase errors are all smaller.

In our research, we are only concerned with phase velocity errors. For completeness, however, we have derived the normalized compressional group velocity α_{gr}/α and shear group velocity β_{gr}/β :

$$\frac{\alpha_{gr}}{\alpha} = \frac{1}{4\mathcal{E}\omega_\alpha} \left[(1+R^2)(\mathcal{E}_{xx,k} + \mathcal{E}_{zz,k}) + (1-R^2) \right. \\ \left. \times \frac{(\mathcal{E}_{xx} - \mathcal{E}_{zz})(\mathcal{E}_{xx,k} - \mathcal{E}_{zz,k}) + 4\mathcal{E}_{xz}\mathcal{E}_{xz,k}}{\sqrt{(\mathcal{E}_{xx} - \mathcal{E}_{zz})^2 + 4\mathcal{E}_{xz}^2}} \right] \\ - \frac{\mathcal{E}_k}{4\mathcal{E}^2\omega_\alpha} \left[(1+R^2)(\mathcal{E}_{xx} + \mathcal{E}_{zz}) \right. \\ \left. + (1-R^2)\sqrt{(\mathcal{E}_{xx} - \mathcal{E}_{zz})^2 + 4\mathcal{E}_{xz}^2} \right], \quad (27)$$

$$\frac{\beta_{gr}}{\beta} = \frac{1}{4\mathcal{E}\omega_\beta} \left[\left(1 + \frac{1}{R^2}\right)(\mathcal{E}_{xx,k} + \mathcal{E}_{zz,k}) + \left(1 - \frac{1}{R^2}\right) \right. \\ \left. \times \frac{(\mathcal{E}_{xx} - \mathcal{E}_{zz})(\mathcal{E}_{xx,k} - \mathcal{E}_{zz,k}) + 4\mathcal{E}_{xz}\mathcal{E}_{xz,k}}{\sqrt{(\mathcal{E}_{xx} - \mathcal{E}_{zz})^2 + 4\mathcal{E}_{xz}^2}} \right] \\ - \frac{\mathcal{E}_k}{4\mathcal{E}^2\omega_\beta} \left[\left(1 + \frac{1}{R^2}\right)(\mathcal{E}_{xx} + \mathcal{E}_{zz}) + \left(1 - \frac{1}{R^2}\right) \right. \\ \left. \times \sqrt{(\mathcal{E}_{xx} - \mathcal{E}_{zz})^2 + 4\mathcal{E}_{xz}^2} \right], \quad (28)$$

where

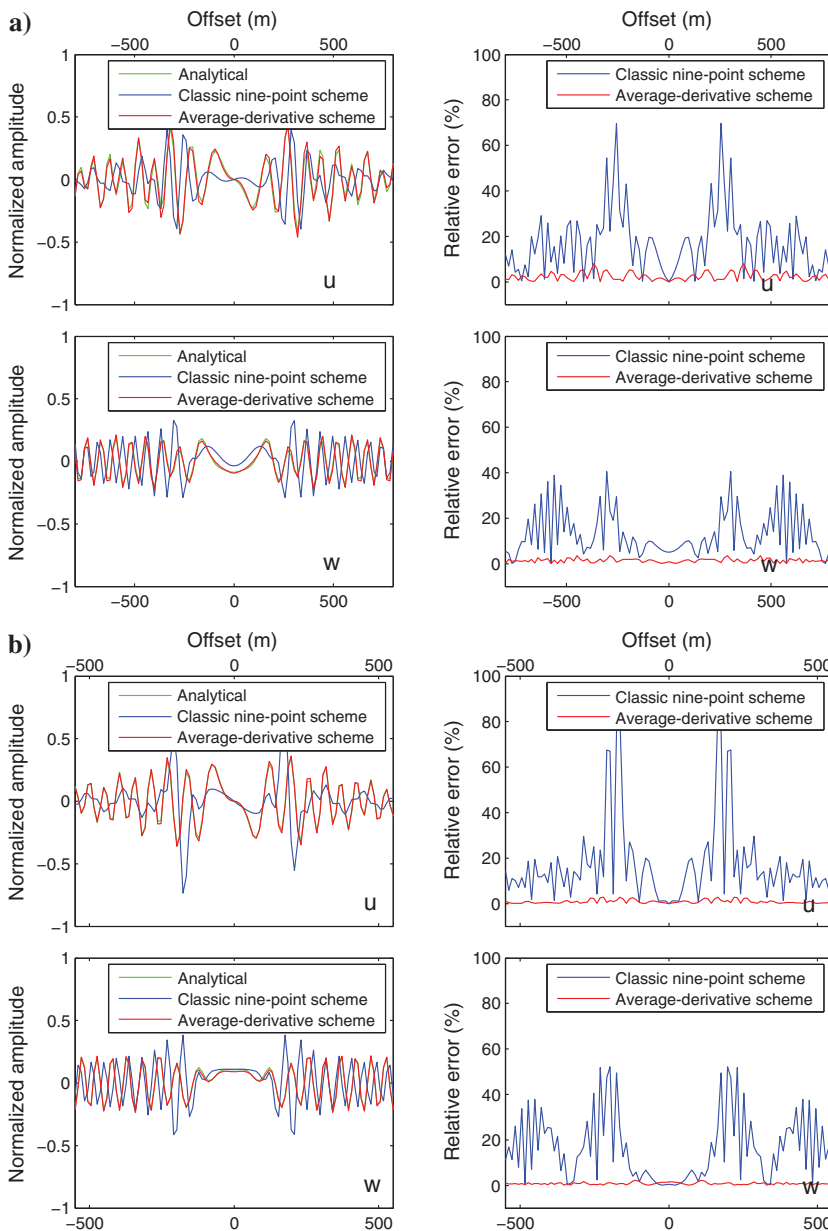


Figure 10. Frequency-domain seismograms ($\omega = 60\pi$) computed with the analytical formula (green line), the classic nine-point scheme (blue line), and the average-derivative scheme (red line). (a) $\sigma = 0.25$ and (b) $\sigma = 0.4$. Here, $\Delta x/\Delta z = 1$.

$$\omega_\alpha = \left\{ \frac{1}{2\mathcal{E}} \left[(1+R^2)(\mathcal{E}_{xx} + \mathcal{E}_{zz}) + (1-R^2)\sqrt{(\mathcal{E}_{xx} - \mathcal{E}_{zz})^2 + 4\mathcal{E}_{xz}^2} \right] \right\}^{\frac{1}{2}},$$

$$\omega_\beta = \left\{ \frac{1}{2\mathcal{E}} \left[\left(1 + \frac{1}{R^2}\right)(\mathcal{E}_{xx} + \mathcal{E}_{zz}) + \left(1 - \frac{1}{R^2}\right)\sqrt{(\mathcal{E}_{xx} - \mathcal{E}_{zz})^2 + 4\mathcal{E}_{xz}^2} \right] \right\}^{\frac{1}{2}},$$

$$\mathcal{E}_k = -2d \left[\sin(k_x \Delta x) \sin \theta + \frac{\sin(k_z \Delta z) \cos \theta}{r} \right] - 4e \sin(k_x \Delta x) \cos(k_z \Delta z) \\ \times \sin \theta - \frac{4e}{r} \cos(k_x \Delta x) \sin(k_z \Delta z) \cos \theta,$$

$$\mathcal{E}_{xx,k} = -\frac{1-\gamma_1}{r} \sin(k_z \Delta z) \cos \theta [2 - 2 \cos(k_x \Delta x)] \\ + 2[(1-\gamma_1) \cos(k_z \Delta z) + \gamma_1] \sin(k_x \Delta x) \sin \theta,$$

$$\mathcal{E}_{zz,k} = -r^2 (1-\gamma_2) \sin(k_x \Delta x) \sin \theta [2 - 2 \cos(k_z \Delta z)] \\ + 2r[(1-\gamma_2) \cos(k_x \Delta x) + \gamma_2] \sin(k_z \Delta z) \cos \theta,$$

$$\mathcal{E}_{xz,k} = r \cos(k_x \Delta x) \sin(k_z \Delta z) \sin \theta + \sin(k_x \Delta x) \cos(k_z \Delta z) \cos \theta. \quad (29)$$

Compared with the phase velocity, the group velocity has larger errors. The average-derivative optimal nine-point scheme still has smaller errors in comparison with the classical nine-point scheme. Because we mainly deal with the phase velocity, we have not shown the results here.

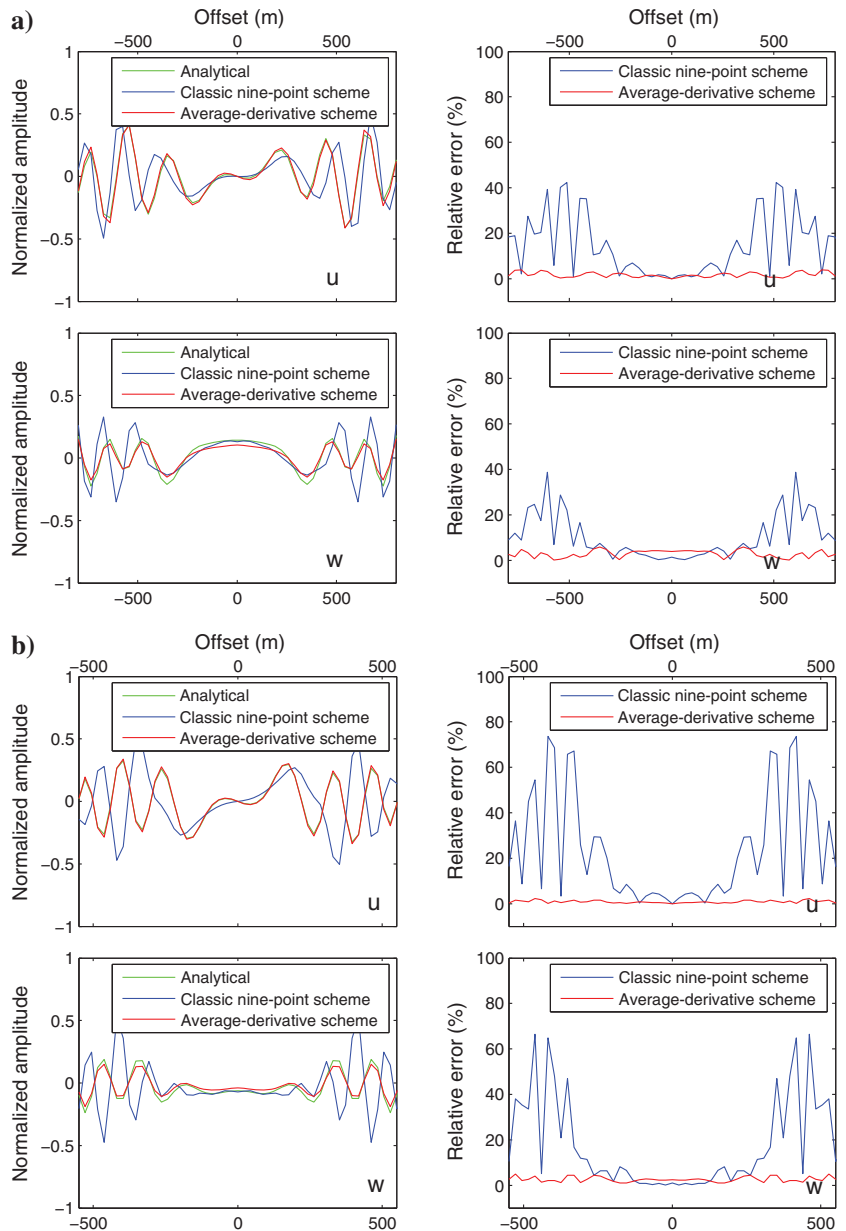
NUMERICAL EXAMPLES

In this section, numerical examples are presented to make comparisons between the average-derivative optimal nine-point scheme and the classic nine-point scheme.

A homogeneous model

We first consider a homogeneous velocity model for which an analytical solution is available. The P-wave velocity is 3500 m/s. We

Figure 11. Frequency-domain seismograms ($\omega = 30\pi$) computed with the analytical formula (green line), the classic nine-point scheme (blue line), and the average-derivative scheme (red line). (a) $\sigma = 0.25$ and (b) 0.4. Here, $\Delta x/\Delta z = 2$.



take a constant density $\rho = 2000 \text{ kg/m}^3$. For the Poisson's ratio, we take $\sigma = 0.25$ and 0.4 , respectively. The corresponding S-wave velocities are 2021 and 1429 m/s , respectively. The numbers of horizontal and vertical grid points are both 101 . To make a comparison with the analytical solution in the full space, perfectly matched layer (PML) boundary conditions are used on the four sides of the computational domain (Appendix B). Figure 8 shows the schematic of the homogeneous model.

We compute the frequency-domain numerical solutions and compare them with the analytical solution (Min et al., 2000). First, we take the circular frequency ω to be 30π . According to the criterion of four grid points per shear wavelength, the sampling intervals for $\sigma = 0.25$ and 0.4 are 32 and 22 m , respectively. A single vertical

force is applied at the center of the model with a Ricker wavelet time history, and a receiver array is placed at the 17th layer in the z -direction. Second, the circular frequency ω is taken to be 60π . According to the criterion of four grid points per shear wavelength, the sampling intervals for $\sigma = 0.25$ and 0.4 are 16 and 11 m , respectively. A receiver array is placed at the 34th layer in the z -direction.

Figures 9 and 10 show frequency-domain seismograms (u and w) computed with the analytic formula, the classical nine-point scheme, and the average-derivative optimal nine-point scheme for $\omega = 30\pi$ and 60π , respectively, where $r = \Delta x/\Delta z = 1$. The relative errors of the two nine-point schemes in comparison with the analytical solution are also displayed. Figures 11 and 12 show the correspond-

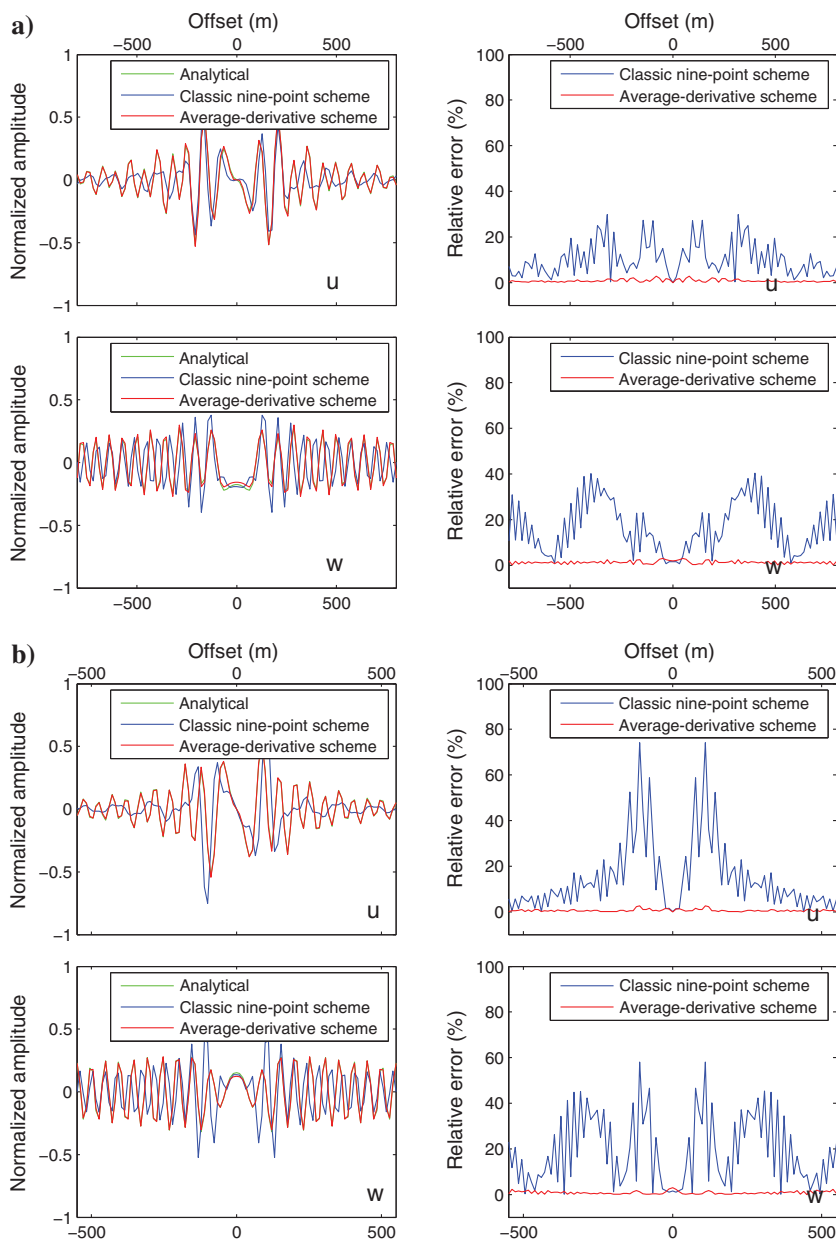


Figure 12. Frequency-domain seismograms ($\omega = 60\pi$) computed with the analytical formula (green line), the classic nine-point scheme (blue line), and the average-derivative scheme (red line). (a) $\sigma = 0.25$ and (b) 0.4 . Here, $\Delta x/\Delta z = 2$.

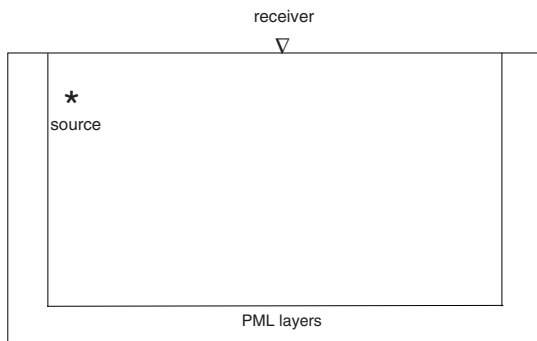


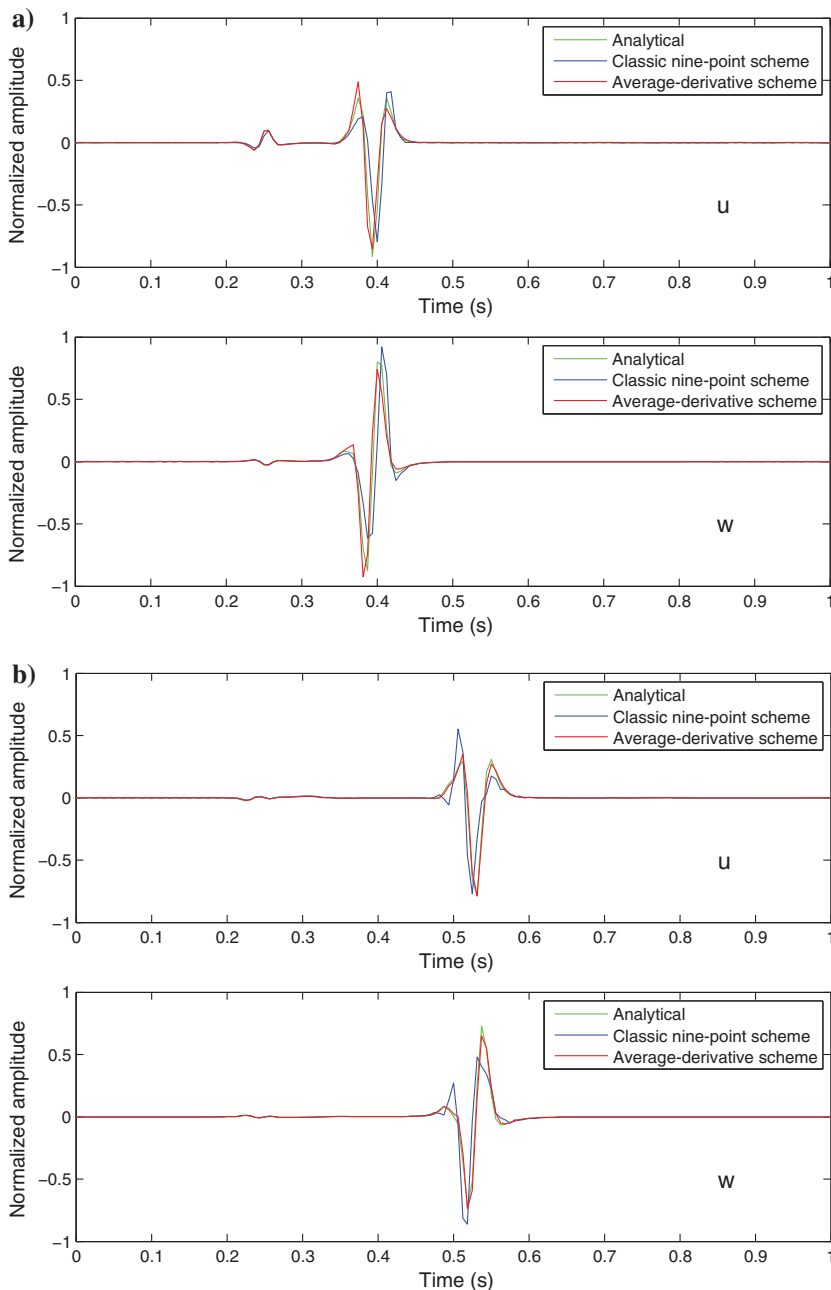
Figure 13. Schematic of the half-space model.

ing results for the case in which $r = \Delta x / \Delta z = 2$. From these figures, we can see that the results of the average-derivative optimal nine-point scheme are in relatively good agreement with the analytical results. The results of the classic nine-point scheme exhibit large errors due to numerical dispersion. It should be noted that the computational cost of the classic nine-point scheme and the average-derivative optimal nine-point scheme is approximately the same.

Lamb’s problem

To address Lamb’s problem, a proper numerical treatment of the free-surface boundary condition is essential. In our example, we use

Figure 14. Time-domain seismograms of Lamb’s problem computed with the analytical solution (green line), the classic nine-point scheme (blue line), and the average-derivative optimal nine-point scheme (red line) at the free-surface with an offset of 660 m: Poisson’s ratio (a) $\sigma = 0.25$ and (b) $\sigma = 0.4$.



an improved free-surface expression presented in Cao et al. (2016). This improved free-surface expression is based on the parameter-modified expression for the free surface (Mittet, 2002; Xu et al., 2007). The analytical solution is calculated with the Cagniard-de Hoop method (Aki and Richards, 1980).

A finite-size model of 1200×240 m is considered in our computation. We take two Poisson's ratios $\sigma = 0.25$ and 0.4 . The corresponding grid intervals are $\Delta x = 6$ m, $\Delta z = 6$ m and $\Delta x = 4$ m, $\Delta z = 4$ m, respectively. To simulate wave propagation in the half-space, PML boundary conditions are used on the other three sides of the model (Figure 13). A single vertical force is applied at the depth of 48 m. Figure 14 shows the time-domain seismograms (u and w) computed with the analytic solution, the classical nine-point scheme, and the average-derivative optimal nine-point scheme at the free-surface with an offset of 660 m. In comparison with the classical nine-point scheme, the average-derivative optimal nine-point scheme agrees with the analytical solution better. The remaining errors are probably due to the inaccuracies in numerical treatment of the free-surface boundary condition.

Overthrust model

We now consider part of the overthrust model with a Poisson's ratio of 0.25 and a constant density of 2300 kg/m^3 (Figure 15). On the top side, we use a centered finite-difference free-surface boundary condition (Alterman and Karal, 1968). For the remaining three sides, PML boundary conditions are applied. The numbers of horizontal and vertical grid points are $n_x = 275$ and $n_z = 75$, respectively. We take $\Delta x = 10$ m and $\Delta z = 5$ m. A single vertical force with a Ricker wavelet time history is applied at $(x = 1370 \text{ m and } z = 50 \text{ m})$. Two receiver lines are set at the depth of 30 and 180 m. The circular frequency ω is taken to be 60π .

For this model, an analytic solution is not available. To make comparisons, we use a method of finer grids. Figure 16 shows frequency-domain seismograms (u and w) at receiver line 1 computed with the classic nine-point scheme with $\Delta x = 10$ m and $\Delta z = 5$ m, the classic nine-point scheme with $\Delta x = 5$ m and $\Delta z = 2.5$ m, and the average-derivative optimal nine-point scheme with $\Delta x = 10$ m and $\Delta z = 5$ m. Figure 17 shows the corresponding results at receiver line 2. We can see that the results of the average-derivative

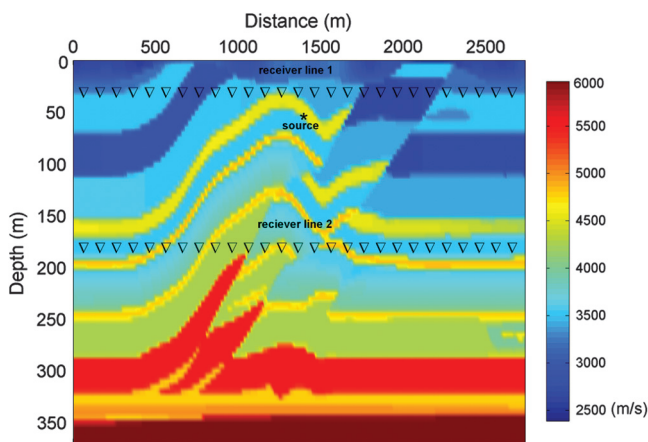


Figure 15. Part of the overthrust model (P-wave velocity). We take $\sigma = 0.25$ and a constant density $\rho = 2000 \text{ kg/m}^3$.

optimal nine-point scheme on a coarse grid are closer to those of the classic nine-point scheme on a fine grid. This demonstrates that the average-derivative optimal nine-point scheme is more accurate than the classical nine-point scheme when these two schemes are computed on the grid with the same grid intervals.

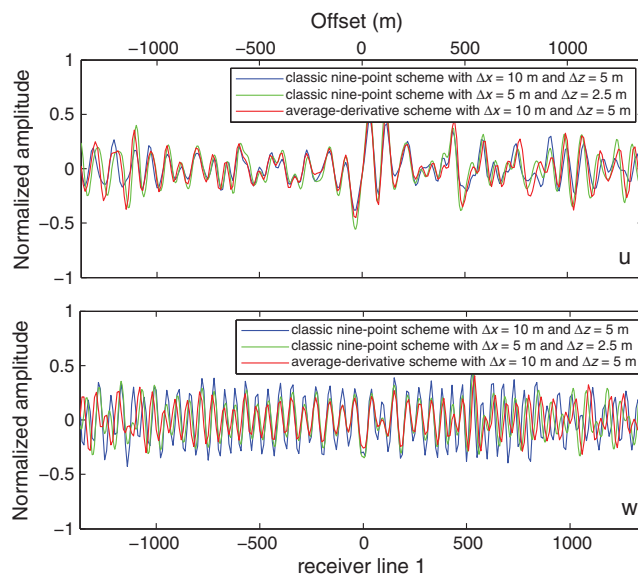


Figure 16. Frequency-domain seismograms (upper plot: u and lower plot: w) at receiver line 1 computed with the classic nine-point scheme with $\Delta x = 10$ m and $\Delta z = 5$ m (blue line), the classic nine-point scheme with $\Delta x = 5$ m and $\Delta z = 2.5$ m (green line), and the average-derivative scheme with $\Delta x = 10$ m and $\Delta z = 5$ m (red line).

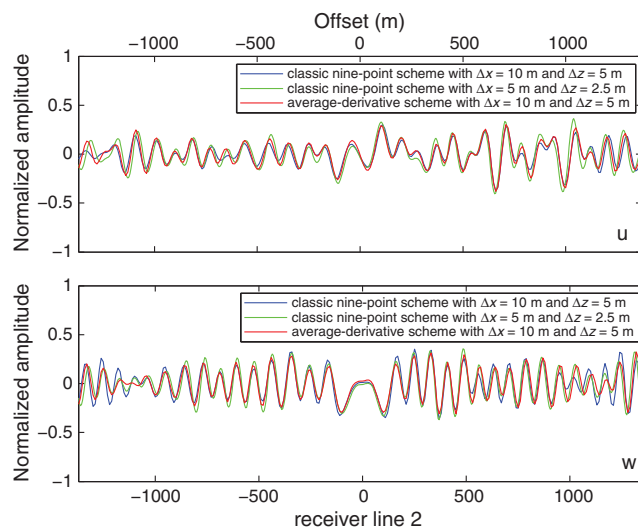


Figure 17. Frequency-domain seismograms (upper plot: u and lower plot: w) at receiver line 2 computed with the classic nine-point scheme with $\Delta x = 10$ m and $\Delta z = 5$ m (blue line), the classic nine-point scheme with $\Delta x = 5$ m and $\Delta z = 2.5$ m (green line), and the average-derivative scheme with $\Delta x = 10$ m and $\Delta z = 5$ m (red line).

Salt model

We now consider a salt model that contains various Poisson's ratios including $\sigma = 0.5$. Figure 18 shows the P-wave velocity, S-wave velocity, density, and Poisson's ratio of the model (House et al., 2000). The parameters of this salt model are $n_x = n_z = 251$, $\Delta x = 5$ m, and $\Delta z = 4$ m. The optimization coefficients for this directional grid interval are listed in Table 2. For a Poisson's ratio that is not covered in Table 2, we use linear interpolation to obtain the corresponding optimization coefficients. An explosive Ricker source with peak frequency of 15 Hz is applied at ($x = 625$ m and $z = 120$ m), and a receiver array is set at the depth of 40 m.

Figure 19 shows monochromatic wavefields of 15 and 30 Hz computed with the classic nine-point scheme and the average-derivative optimal nine-point scheme. Due to the spurious S-waves generated by the classical nine-point scheme, the wavefields computed with the classical nine-point scheme exhibit badly contaminated results in the water, particularly for the wavefield of 15 Hz. These spurious S-waves are a kind of artifacts produced by numerical discretizations. The reason why we call them spurious S-waves is because these artifacts stem from the S-wave numerical dispersion relation of the classical nine-point scheme when the Poisson's ratio is 0.5. On the other hand, the wavefields computed with the average-derivative optimal nine-point scheme show clean results in the water. This is because the numerical S-wave phase velocity of the average-derivative optimal nine-point scheme becomes zero in the water. We show the time-domain seismograms computed with the classic nine-point scheme and the average-derivative optimal nine-point scheme in Figure 20. These time-domain seismograms are obtained by temporal Fourier transform of frequency-domain wavefields. In comparison with the seismogram computed with the average-derivative optimal nine-point scheme, the seismogram computed with the classical nine-point scheme is dominated by low-velocity spurious S-waves and thus become unacceptable.

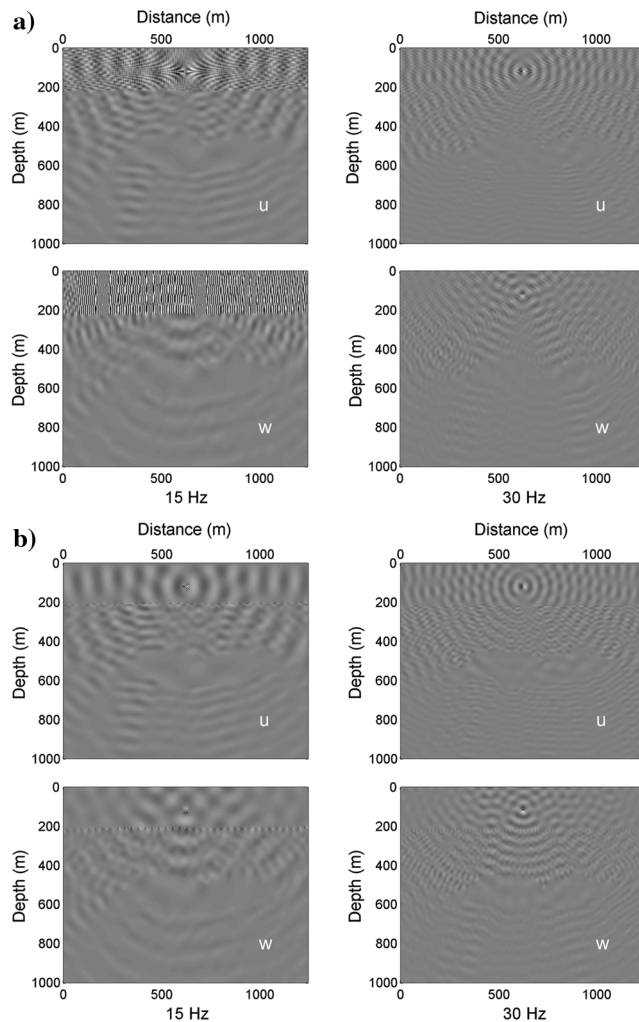
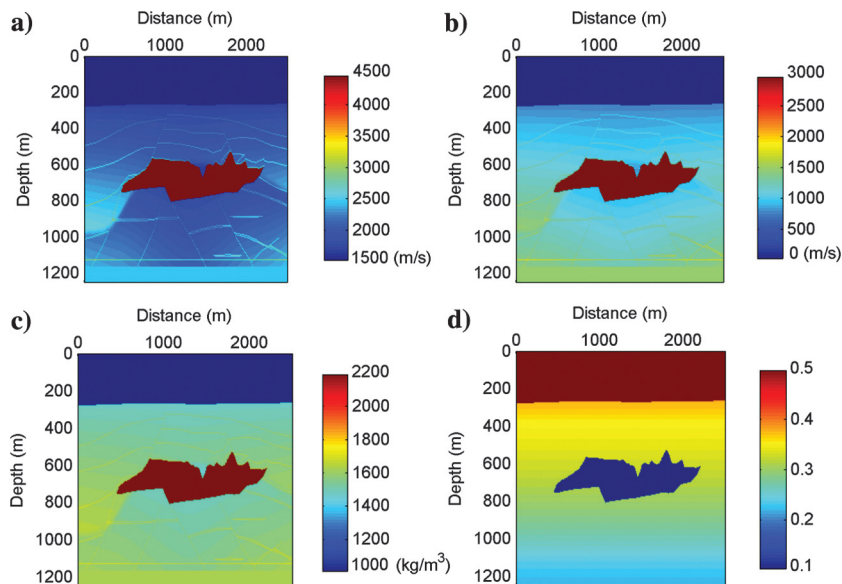


Figure 19. (a) Monochromatic wavefields of the salt model computed with the classic nine-point scheme and (b) the average-derivative optimal nine-point scheme.

Figure 18. The salt model: (a) P-wave velocity, (b) S-wave velocity, (c) density, and (d) Poisson's ratio.



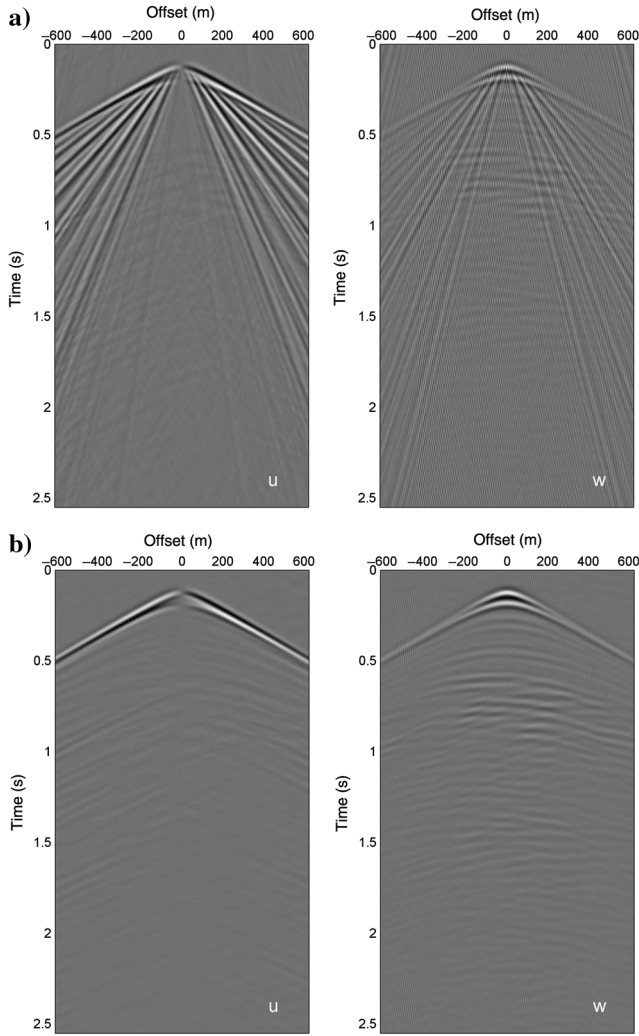


Figure 20. (a) Time-domain seismograms computed with the classic nine-point scheme and (b) the average-derivative optimal nine-point scheme.

CONCLUSIONS

We have developed an average-derivative optimal nine-point scheme for frequency domain 2D elastic-wave equation. Compared with the classical nine-point scheme, this new nine-point scheme reduces the number of grid points per shear wavelength from 10 or 20 to 4 for $\sigma = 0.25$ or 0.4 . For $\sigma = 0.5$, the S-wave phase velocity of the new nine-point scheme is zero, whereas the classical nine-point scheme produces spurious S-waves. These conclusions apply to arbitrary directional grid intervals. Numerical examples demonstrate that the new nine-point scheme produces more accurate modeling results in comparison with the classical nine-point scheme at approximately the same computational cost. This new nine-point scheme is also generalized to an average-derivative 27-point scheme for frequency-domain 3D elastic-wave equation.

ACKNOWLEDGMENTS

We would like to thank the anonymous reviewers for valuable suggestions. This work is supported by National Natural Science Foundation of China under grant nos. 41474104 and 41274139.

APPENDIX A

3D CASE

We consider the 3D elastic-wave equation in the frequency domain

$$\begin{aligned} \frac{\partial}{\partial x} \left(\eta \frac{\partial u}{\partial x} \right) + \frac{\partial}{\partial y} \left(\mu \frac{\partial u}{\partial y} \right) + \frac{\partial}{\partial z} \left(\mu \frac{\partial u}{\partial z} \right) + \frac{\partial}{\partial x} \left(\lambda \frac{\partial v}{\partial y} \right) \\ + \frac{\partial}{\partial y} \left(\mu \frac{\partial v}{\partial x} \right) + \frac{\partial}{\partial x} \left(\lambda \frac{\partial w}{\partial z} \right) + \frac{\partial}{\partial z} \left(\mu \frac{\partial w}{\partial x} \right) + \rho \omega^2 u = 0, \end{aligned} \quad (\text{A-1})$$

$$\begin{aligned} \frac{\partial}{\partial x} \left(\mu \frac{\partial v}{\partial x} \right) + \frac{\partial}{\partial y} \left(\eta \frac{\partial v}{\partial y} \right) + \frac{\partial}{\partial z} \left(\mu \frac{\partial v}{\partial z} \right) + \frac{\partial}{\partial y} \left(\lambda \frac{\partial w}{\partial z} \right) \\ + \frac{\partial}{\partial z} \left(\mu \frac{\partial w}{\partial y} \right) + \frac{\partial}{\partial y} \left(\lambda \frac{\partial u}{\partial x} \right) + \frac{\partial}{\partial x} \left(\mu \frac{\partial u}{\partial y} \right) + \rho \omega^2 v = 0, \end{aligned} \quad (\text{A-2})$$

$$\begin{aligned} \frac{\partial}{\partial x} \left(\mu \frac{\partial w}{\partial x} \right) + \frac{\partial}{\partial y} \left(\mu \frac{\partial w}{\partial y} \right) + \frac{\partial}{\partial z} \left(\eta \frac{\partial w}{\partial z} \right) + \frac{\partial}{\partial z} \left(\lambda \frac{\partial u}{\partial x} \right) \\ + \frac{\partial}{\partial x} \left(\mu \frac{\partial u}{\partial z} \right) + \frac{\partial}{\partial z} \left(\lambda \frac{\partial v}{\partial y} \right) + \frac{\partial}{\partial y} \left(\mu \frac{\partial v}{\partial z} \right) + \rho \omega^2 w = 0, \end{aligned} \quad (\text{A-3})$$

where u , v , and w are the particle displacements in the x -, y -, and z -directions, respectively.

Using the same approach as the 2D case, an average-derivative 27-point scheme for equations A-1–A-3 can be obtained as follows:

$$\begin{aligned} \frac{1}{\Delta x^2} \left[\eta_{m+\frac{1}{2},l,n} \tilde{u}_{m+1,l,n} - \left(\eta_{m+\frac{1}{2},l,n} + \eta_{m-\frac{1}{2},n} \right) \tilde{u}_{m,n} + \eta_{m-\frac{1}{2},l,n} \tilde{u}_{m-1,l,n} \right] \\ + \frac{1}{\Delta y^2} \left[\mu_{m,l,n+\frac{1}{2}} \hat{u}_{m,l+1,n} - \left(\mu_{m,l+\frac{1}{2},n} + \mu_{m,l-\frac{1}{2},n} \right) \hat{u}_{m,l,n} + \mu_{m,l-\frac{1}{2},n} \hat{u}_{m,l-1,n} \right] \\ + \frac{1}{\Delta z^2} \left[\mu_{m,l,n+\frac{1}{2}} \tilde{u}_{m,l,n+1} - \left(\mu_{m,l,n+\frac{1}{2}} + \mu_{m,l,n-\frac{1}{2}} \right) \tilde{u}_{m,l,n} + \mu_{m,l,n-\frac{1}{2}} \tilde{u}_{m,l,n-1} \right] \\ + \frac{1}{4\Delta x \Delta y} \left[\lambda_{m+1,l,n} (w_{m+1,l+1,n} - w_{m+1,l-1,n}) - \lambda_{m-1,l,n} (w_{m-1,l+1,n} - w_{m-1,l-1,n}) \right] \\ + \frac{1}{4\Delta x \Delta y} \left[\mu_{m,l+1,n} (w_{m+1,l+1,n} - w_{m-1,l+1,n}) - \mu_{m,l-1,n} (w_{m+1,l-1,n} - w_{m-1,l-1,n}) \right] \\ + \frac{1}{4\Delta x \Delta z} \left[\lambda_{m+1,l,n} (w_{m+1,l,n+1} - w_{m+1,l,n-1}) - \lambda_{m-1,l,n} (w_{m-1,l,n+1} - w_{m-1,l,n-1}) \right] \\ + \frac{1}{4\Delta x \Delta z} \left[\mu_{m,n+1} (w_{m+1,l,n+1} - w_{m-1,l,n+1}) - \mu_{m,l,n-1} (w_{m+1,l,n-1} - w_{m-1,l,n-1}) \right] \\ + \rho_{m,l,n} \omega^2 (c u_{m,l,n} + d A + e B + f C) = 0, \end{aligned} \quad (\text{A-4})$$

$$\begin{aligned}
& \frac{1}{\Delta x^2} \left[\mu_{m+\frac{1}{2},l,n} \bar{v}_{m+1,l,n} - \left(\mu_{m+\frac{1}{2},l,n} + \mu_{m-\frac{1}{2},n} \right) \bar{v}_{m,n} + \eta_{m-\frac{1}{2},l,n} \bar{u}_{m-1,l,n} \right] \\
& + \frac{1}{\Delta y^2} \left[\eta_{m,l,n+\frac{1}{2}} \hat{v}_{m,l+1,n} - \left(\eta_{m,l,n+\frac{1}{2}} + \eta_{m,l,n-\frac{1}{2}} \right) \hat{v}_{m,l,n} + \mu_{m,l-\frac{1}{2},n} \hat{v}_{m,l-1,n} \right] \\
& + \frac{1}{\Delta z^2} \left[\mu_{m,l,n+\frac{1}{2}} \tilde{v}_{m,l,n+1} - \left(\mu_{m,l,n+\frac{1}{2}} + \mu_{m,l,n-\frac{1}{2}} \right) \tilde{v}_{m,l,n} + \mu_{m,l,n-\frac{1}{2}} \tilde{v}_{m,l,n-1} \right] \\
& + \frac{1}{4\Delta y\Delta z} [\lambda_{m,l+1,n} (w_{m,l+1,n+1} - w_{m,l+1,n-1}) - \lambda_{m,l-1,n} (w_{m,l-1,n+1} - w_{m,l-1,n-1})] \\
& + \frac{1}{4\Delta z\Delta y} [\mu_{m,l,n+1} (w_{m,l+1,n+1} - w_{m,l-1,n+1}) - \mu_{m,l,n-1} (w_{m,l+1,n-1} - w_{m,l-1,n-1})] \\
& + \frac{1}{4\Delta y\Delta x} [\lambda_{m,l+1,n} (u_{m+1,l+1,n} - u_{m-1,l+1,n}) - \lambda_{m,l-1,n} (u_{m+1,l-1,n} - u_{m-1,l-1,n})] \\
& + \frac{1}{4\Delta x\Delta y} [\mu_{m+1,l,n} (u_{m+1,l+1,n} - u_{m+1,l-1,n}) - \mu_{m-1,l,n} (u_{m-1,l+1,n} - u_{m-1,l-1,n})] \\
& + \rho_{m,l,n} \omega^2 (c v_{m,l,n} + dA + eB + fC) = 0, \tag{A-5}
\end{aligned}$$

$$\begin{aligned}
& \frac{1}{\Delta x^2} \left[\mu_{m+\frac{1}{2},l,n} \bar{w}_{m+1,l,n} - \left(\mu_{m+\frac{1}{2},l,n} + \mu_{m-\frac{1}{2},n} \right) \bar{w}_{m,n} + \mu_{m-\frac{1}{2},l,n} \bar{w}_{m-1,l,n} \right] \\
& + \frac{1}{\Delta y^2} \left[\mu_{m,l,n+\frac{1}{2}} \hat{w}_{m,l+1,n} - \left(\mu_{m,l,n+\frac{1}{2}} + \mu_{m,l,n-\frac{1}{2}} \right) \hat{w}_{m,l,n} + \mu_{m,l-\frac{1}{2},n} \hat{w}_{m,l-1,n} \right] \\
& + \frac{1}{\Delta z^2} \left[\eta_{m,l,n+\frac{1}{2}} \tilde{w}_{m,l,n+1} - \left(\eta_{m,l,n+\frac{1}{2}} + \eta_{m,l,n-\frac{1}{2}} \right) \tilde{w}_{m,l,n} + \eta_{m,l,n-\frac{1}{2}} \tilde{w}_{m,l,n-1} \right] \\
& + \frac{1}{4\Delta z\Delta x} [\lambda_{m+1,l,n} (u_{m+1,l,n+1} - u_{m-1,l,n+1}) - \lambda_{m-1,l,n} (u_{m+1,l,n-1} - u_{m-1,l,n-1})] \\
& + \frac{1}{4\Delta x\Delta z} [\mu_{m+1,l,n} (u_{m+1,l,n+1} - u_{m+1,l,n-1}) - \mu_{m-1,l,n} (u_{m-1,l,n+1} - u_{m-1,l,n-1})] \\
& + \frac{1}{4\Delta z\Delta y} [\lambda_{m,l,n+1} (v_{m,l+1,n+1} - v_{m,l-1,n+1}) - \lambda_{m,l-1,n} (v_{m,l+1,n-1} - v_{m,l-1,n-1})] \\
& + \frac{1}{4\Delta y\Delta z} [\mu_{m,l+1,n} (v_{m,l+1,n+1} - v_{m,l+1,n-1}) - \mu_{m,l-1,n} (v_{m,l-1,n+1} - v_{m,l-1,n-1})] \\
& + \rho_{m,l,n} \omega^2 (c w_{m,l,n} + dA + eB + fC) = 0, \tag{A-6}
\end{aligned}$$

where

$$\begin{aligned}
\bar{p}_{m+j,l,n} &= \alpha_1 (p_{m+j,l+1,n} + p_{m+j,l,n+1} + p_{m+j,l-1,n} + p_{m+j,l,n-1}) \\
& + \alpha_2 (p_{m+j,l+1,n+1} + p_{m+j,l-1,n+1} + p_{m+j,l+1,n-1} + p_{m+j,l-1,n-1}) \\
& + (1 - 4\alpha_1 - 4\alpha_2) p_{m+j,l,n}, \quad j = -1, 0, 1, \\
\hat{p}_{m,l+j,n} &= \beta_1 (p_{m+1,l+j,n} + p_{m,l+j,n+1} + p_{m-1,l+j,n} + p_{m,l+j,n-1}) \\
& + \beta_2 (p_{m+1,l+j,n+1} + p_{m+1,l+j,n-1} + p_{m-1,l+j,n+1} + p_{m-1,l+j,n-1}) \\
& + (1 - 4\beta_1 - 4\beta_2) p_{m,l+j,n}, \quad j = -1, 0, 1, \\
\tilde{p}_{m,l,n+j} &= \gamma_1 (p_{m+1,l,n+j} + p_{m,l+1,n+j} + p_{m-1,l,n+j} + p_{m,l-1,n+j}) \\
& + \gamma_2 (p_{m+1,l+1,n+j} + p_{m+1,l-1,n+j} + p_{m-1,l+1,n+j} + p_{m-1,l-1,n+j}) \\
& + (1 - 4\gamma_1 - 4\gamma_2) p_{m,l,n+j}, \quad j = -1, 0, 1, \\
A &= (p_{m,l+1,n} + p_{m,l,n+1} + p_{m,l-1,n} + p_{m,l,n-1} + p_{m+1,l,n} + p_{m-1,l,n}), \\
B &= (p_{m+1,l+1,n} + p_{m+1,l,n+1} + p_{m+1,l-1,n} + p_{m+1,l,n-1} + p_{m-1,l+1,n} + p_{m-1,l,n+1} \\
& + p_{m-1,l-1,n} + p_{m-1,l,n-1} + p_{m,l+1,n+1} + p_{m,l-1,n+1} + p_{m,l+1,n-1} + p_{m,l-1,n-1}), \\
C &= (p_{m+1,l+1,n+1} + p_{m+1,l-1,n+1} + p_{m+1,l+1,n-1} + p_{m+1,l-1,n-1} \\
& + p_{m-1,l+1,n+1} + p_{m-1,l-1,n+1} + p_{m-1,l+1,n-1} + p_{m-1,l-1,n-1}), \tag{A-7}
\end{aligned}$$

where p represents u , v , or w , and α_1 , α_2 , β_1 , β_2 , γ_1 , γ_2 , c , d , and e are coefficients. Here, $f = (1 - c - 6d - 12e)/8$.

APPENDIX B

IMPLEMENTATION OF PML BOUNDARY CONDITIONS

The 2D frequency-domain elastic-wave equations with PML boundary conditions are

$$\begin{aligned}
& \frac{1}{\xi_x} \frac{\partial}{\partial x} \left(\frac{\eta}{\xi_x} \frac{\partial u}{\partial x} \right) + \frac{1}{\xi_z} \frac{\partial}{\partial z} \left(\frac{\mu}{\xi_z} \frac{\partial u}{\partial z} \right) + \frac{1}{\xi_x} \frac{\partial}{\partial x} \left(\frac{\lambda}{\xi_z} \frac{\partial w}{\partial z} \right) \\
& + \frac{1}{\xi_z} \frac{\partial}{\partial z} \left(\frac{\mu}{\xi_x} \frac{\partial w}{\partial x} \right) + \rho \omega^2 u = 0, \tag{B-1}
\end{aligned}$$

$$\begin{aligned}
& \frac{1}{\xi_x} \frac{\partial}{\partial x} \left(\frac{\mu}{\xi_x} \frac{\partial w}{\partial x} \right) + \frac{1}{\xi_z} \frac{\partial}{\partial z} \left(\frac{\eta}{\xi_z} \frac{\partial w}{\partial z} \right) + \frac{1}{\xi_x} \frac{\partial}{\partial x} \left(\frac{\mu}{\xi_z} \frac{\partial u}{\partial z} \right) \\
& + \frac{1}{\xi_z} \frac{\partial}{\partial z} \left(\frac{\lambda}{\xi_x} \frac{\partial u}{\partial x} \right) + \rho \omega^2 w = 0, \tag{B-2}
\end{aligned}$$

where

$$\xi_x(x) = 1 - \frac{ic_x}{\omega} \cos\left(\frac{\pi x}{2L_x}\right), \tag{B-3}$$

$$\xi_z(z) = 1 - \frac{ic_z}{\omega} \cos\left(\frac{\pi z}{2L_z}\right), \tag{B-4}$$

where L_x and L_z denote the width of the PML layer in x - and z -directions, respectively. The coordinates x and z are local coordinates whose origins are located at the outer edges of the PML layers. The scalars c_x and c_z are determined by trial and error (Operto et al., 2007).

The corresponding average-derivative optimal nine-point scheme becomes

$$\begin{aligned}
& \frac{1}{\xi_{x_m} \Delta x^2} \left[\frac{\eta_{m+\frac{1}{2},n}}{\xi_{x_{m+\frac{1}{2}}}} \bar{u}_{m+1,n} - \left(\frac{\eta_{m+\frac{1}{2},n}}{\xi_{x_{m+\frac{1}{2}}}} + \frac{\eta_{m-\frac{1}{2},n}}{\xi_{x_{m-\frac{1}{2}}}} \right) \bar{u}_{m,n} + \frac{\eta_{m-\frac{1}{2},n}}{\xi_{x_{m-\frac{1}{2}}}} \bar{u}_{m-1,n} \right] \\
& + \frac{1}{\xi_{z_n} \Delta z^2} \left[\frac{\mu_{m,n+\frac{1}{2}}}{\xi_{z_{n+\frac{1}{2}}}} \tilde{u}_{m,n+1} - \left(\frac{\mu_{m,n+\frac{1}{2}}}{\xi_{z_{n+\frac{1}{2}}}} + \frac{\mu_{m,n-\frac{1}{2}}}{\xi_{z_{n-\frac{1}{2}}}} \right) \tilde{u}_{m,n} + \frac{\mu_{m,n-\frac{1}{2}}}{\xi_{z_{n-\frac{1}{2}}}} \tilde{u}_{m,n-1} \right] \\
& + \frac{1}{4\xi_{x_m} \Delta x \Delta z} \left[\frac{\lambda_{m+1,n}}{\xi_{z_n}} (w_{m+1,n+1} - w_{m+1,n-1}) - \frac{\lambda_{m-1,n}}{\xi_{z_n}} (w_{m-1,n+1} - w_{m-1,n-1}) \right] \\
& + \frac{1}{4\xi_{z_n} \Delta x \Delta z} \left[\frac{\mu_{m,n+1}}{\xi_{x_m}} (w_{m+1,n+1} - w_{m-1,n+1}) - \frac{\mu_{m,n-1}}{\xi_{x_m}} (w_{m+1,n-1} - w_{m-1,n-1}) \right] \\
& + \rho_{m,n} \omega^2 [c u_{m,n} + d(u_{m+1,n} + u_{m-1,n} + u_{m,n+1} + u_{m,n-1}) \\
& + e(u_{m+1,n+1} + u_{m-1,n+1} + u_{m+1,n-1} + u_{m-1,n-1})] = 0, \tag{B-5}
\end{aligned}$$

$$\begin{aligned} & \frac{1}{\xi_{x_m} \Delta x^2} \left[\frac{\mu_{m+\frac{1}{2},n}}{\xi_{x_{m+\frac{1}{2}}}} \tilde{w}_{m+1,n} - \left(\frac{\mu_{m+\frac{1}{2},n}}{\xi_{x_{m+\frac{1}{2}}}} + \frac{\mu_{m-\frac{1}{2},n}}{\xi_{x_{m-\frac{1}{2}}}} \right) \tilde{w}_{m,n} + \frac{\mu_{m-\frac{1}{2},n}}{\xi_{x_{m-\frac{1}{2}}}} \tilde{w}_{m-1,n} \right] \\ & + \frac{1}{\xi_{z_n} \Delta z^2} \left[\frac{\eta_{m,n+\frac{1}{2}}}{\xi_{z_{n+\frac{1}{2}}}} \tilde{w}_{m,n+1} - \left(\frac{\eta_{m,n+\frac{1}{2}}}{\xi_{z_{n+\frac{1}{2}}}} + \frac{\eta_{m,n-\frac{1}{2}}}{\xi_{z_{n-\frac{1}{2}}}} \right) \tilde{w}_{m,n} + \frac{\eta_{m,n-\frac{1}{2}}}{\xi_{z_{n-\frac{1}{2}}}} \tilde{w}_{m,n-1} \right] \\ & + \frac{1}{4\xi_{x_m} \Delta x \Delta z} \left[\frac{\mu_{m+1,n}}{\xi_{z_n}} (u_{m+1,n+1} - u_{m+1,n-1}) - \frac{\mu_{m-1,n}}{\xi_{z_n}} (u_{m-1,n+1} - u_{m-1,n-1}) \right] \\ & + \frac{1}{4\xi_{z_n} \Delta x \Delta z} \left[\frac{\lambda_{m,n+1}}{\xi_{x_m}} (u_{m+1,n+1} - u_{m-1,n+1}) - \frac{\lambda_{m,n-1}}{\xi_{x_m}} (u_{m+1,n-1} - u_{m-1,n-1}) \right] \\ & + \rho_{m,n} \omega^2 [c w_{m,n} + d(w_{m+1,n} + u_{m-1,n} + w_{m,n+1} + w_{m,n-1}) \\ & + e(w_{m+1,n+1} + w_{m-1,n+1} + w_{m+1,n-1} + w_{m-1,n-1})] = 0. \end{aligned} \quad (B-6)$$

We can rewrite schemes B-5 and B-6 as

$$\begin{aligned} & c_1 u_{m-1,n-1} + c_2 u_{m,n-1} + c_3 u_{m+1,n-1} + c_4 u_{m-1,n} + c_5 u_{m,n} \\ & + c_6 u_{m+1,n} + c_7 u_{m-1,n+1} + c_8 u_{m,n+1} + c_9 u_{m+1,n+1} \\ & + d_1 w_{m-1,n-1} + d_2 w_{m+1,n-1} + d_3 w_{m-1,n+1} + d_4 w_{m+1,n+1} = 0, \end{aligned} \quad (B-7)$$

$$\begin{aligned} & \tilde{d}_1 w_{m-1,n-1} + \tilde{d}_2 w_{m,n-1} + \tilde{d}_3 w_{m+1,n-1} + \tilde{d}_4 w_{m-1,n} + \tilde{d}_5 w_{m,n} \\ & + \tilde{d}_6 w_{m+1,n} + \tilde{d}_7 w_{m-1,n+1} + \tilde{d}_8 w_{m,n+1} + \tilde{d}_9 w_{m+1,n+1} \\ & + \tilde{c}_1 u_{m-1,n-1} + \tilde{c}_2 u_{m+1,n-1} + \tilde{c}_3 u_{m-1,n+1} + \tilde{c}_4 u_{m+1,n+1} = 0, \end{aligned} \quad (B-8)$$

where

$$\begin{aligned} c_1 &= \frac{1}{\xi_{x_m} \Delta x^2} \frac{\eta_{m-\frac{1}{2},n} 1 - \gamma_1}{\xi_{x_{m-\frac{1}{2}}}} + \frac{1}{\xi_{z_n} \Delta z^2} \frac{\mu_{m-\frac{1}{2},n} 1 - \gamma_2}{\xi_{z_{n-\frac{1}{2}}}} + \rho_{m,n} \omega^2 e, \\ c_2 &= -\frac{1}{\xi_{x_m} \Delta x^2} \left(\frac{\eta_{m+\frac{1}{2},n}}{\xi_{x_{m+\frac{1}{2}}}} + \frac{\eta_{m-\frac{1}{2},n}}{\xi_{x_{m-\frac{1}{2}}}} \right) \frac{1 - \gamma_1}{2} + \frac{1}{\xi_{z_n} \Delta z^2} \frac{\mu_{m-\frac{1}{2},n}}{\xi_{z_{n-\frac{1}{2}}}} \gamma_2 + \rho_{m,n} \omega^2 d, \\ c_3 &= \frac{1}{\xi_{x_m} \Delta x^2} \frac{\eta_{m+\frac{1}{2},n} 1 - \gamma_1}{\xi_{x_{m+\frac{1}{2}}}} + \frac{1}{\xi_{z_n} \Delta z^2} \frac{\mu_{m-\frac{1}{2},n} 1 - \gamma_2}{\xi_{z_{n-\frac{1}{2}}}} + \rho_{m,n} \omega^2 e, \\ c_4 &= \frac{1}{\xi_{x_m} \Delta x^2} \frac{\eta_{m-\frac{1}{2},n}}{\xi_{x_{m-\frac{1}{2}}}} \gamma_1 - \frac{1}{\xi_{z_n} \Delta z^2} \left(\frac{\mu_{m,n+\frac{1}{2}}}{\xi_{z_{n+\frac{1}{2}}}} + \frac{\mu_{m,n-\frac{1}{2}}}{\xi_{z_{n-\frac{1}{2}}}} \right) \frac{1 - \gamma_2}{2} + \rho_{m,n} \omega^2 d, \\ c_5 &= -\frac{1}{\xi_{x_m} \Delta x^2} \left(\frac{\eta_{m+\frac{1}{2},n}}{\xi_{x_{m+\frac{1}{2}}}} + \frac{\eta_{m-\frac{1}{2},n}}{\xi_{x_{m-\frac{1}{2}}}} \right) \gamma_1 - \frac{1}{\xi_{z_n} \Delta z^2} \left(\frac{\mu_{m,n+\frac{1}{2}}}{\xi_{z_{n+\frac{1}{2}}}} + \frac{\mu_{m,n-\frac{1}{2}}}{\xi_{z_{n-\frac{1}{2}}}} \right) \gamma_2 + \rho_{m,n} \omega^2 c, \\ c_6 &= \frac{1}{\xi_{x_m} \Delta x^2} \frac{\eta_{m+\frac{1}{2},n}}{\xi_{x_{m+\frac{1}{2}}}} \gamma_1 - \frac{1}{\xi_{z_n} \Delta z^2} \left(\frac{\mu_{m,n+\frac{1}{2}}}{\xi_{z_{n+\frac{1}{2}}}} + \frac{\mu_{m,n-\frac{1}{2}}}{\xi_{z_{n-\frac{1}{2}}}} \right) \frac{1 - \gamma_2}{2} + \rho_{m,n} \omega^2 d, \\ c_7 &= \frac{1}{\xi_{x_m} \Delta x^2} \frac{\eta_{m-\frac{1}{2},n} 1 - \gamma_1}{\xi_{x_{m-\frac{1}{2}}}} + \frac{1}{\xi_{z_n} \Delta z^2} \frac{\mu_{m-\frac{1}{2},n} 1 - \gamma_2}{\xi_{z_{n-\frac{1}{2}}}} + \rho_{m,n} \omega^2 e, \\ c_8 &= -\frac{1}{\xi_{x_m} \Delta x^2} \left(\frac{\eta_{m+\frac{1}{2},n}}{\xi_{x_{m+\frac{1}{2}}}} + \frac{\eta_{m-\frac{1}{2},n}}{\xi_{x_{m-\frac{1}{2}}}} \right) \frac{1 - \gamma_1}{2} + \frac{1}{\xi_{z_n} \Delta z^2} \frac{\mu_{m,n+\frac{1}{2}}}{\xi_{z_{n+\frac{1}{2}}}} \gamma_2 + \rho_{m,n} \omega^2 d, \\ c_9 &= \frac{1}{\xi_{x_m} \Delta x^2} \frac{\eta_{m+\frac{1}{2},n} 1 - \gamma_1}{\xi_{x_{m+\frac{1}{2}}}} + \frac{1}{\xi_{z_n} \Delta z^2} \frac{\mu_{m,n+\frac{1}{2}} 1 - \gamma_2}{\xi_{z_{n+\frac{1}{2}}}} + \rho_{m,n} \omega^2 e, \\ d_1 &= \frac{1}{4\xi_{x_m} \Delta x \Delta z} \frac{\lambda_{m-1,n}}{\xi_{z_n}} + \frac{1}{4\xi_{z_n} \Delta x \Delta z} \frac{\mu_{m-1,n}}{\xi_{x_m}}, \\ d_2 &= -\frac{1}{4\xi_{x_m} \Delta x \Delta z} \frac{\lambda_{m+1,n}}{\xi_{z_n}} - \frac{1}{4\xi_{z_n} \Delta x \Delta z} \frac{\mu_{m+1,n}}{\xi_{x_m}}, \end{aligned}$$

$$\begin{aligned} d_3 &= -\frac{1}{4\xi_{x_m} \Delta x \Delta z} \frac{\lambda_{m-1,n}}{\xi_{z_n}} - \frac{1}{4\xi_{z_n} \Delta x \Delta z} \frac{\mu_{m,n+1}}{\xi_{x_m}}, \quad d_4 = \frac{1}{4\xi_{x_m} \Delta x \Delta z} \frac{\lambda_{m+1,n}}{\xi_{z_n}} + \frac{1}{4\xi_{z_n} \Delta x \Delta z} \frac{\mu_{m,n+1}}{\xi_{x_m}}, \\ \tilde{d}_1 &= \frac{1}{\xi_{x_m} \Delta x^2} \frac{\mu_{m-\frac{1}{2},n} 1 - \gamma_1}{\xi_{x_{m-\frac{1}{2}}}} + \frac{1}{\xi_{z_n} \Delta z^2} \frac{\eta_{m,n-\frac{1}{2}} 1 - \gamma_2}{\xi_{z_{n-\frac{1}{2}}}} + \rho_{m,n} \omega^2 e, \\ \tilde{d}_2 &= -\frac{1}{\xi_{x_m} \Delta x^2} \left(\frac{\mu_{m+\frac{1}{2},n}}{\xi_{x_{m+\frac{1}{2}}}} + \frac{\mu_{m-\frac{1}{2},n}}{\xi_{x_{m-\frac{1}{2}}}} \right) \frac{1 - \gamma_1}{2} + \frac{1}{\xi_{z_n} \Delta z^2} \frac{\eta_{m,n-\frac{1}{2}}}{\xi_{z_{n-\frac{1}{2}}}} \gamma_2 + \rho_{m,n} \omega^2 d, \\ \tilde{d}_3 &= \frac{1}{\xi_{x_m} \Delta x^2} \frac{\mu_{m+\frac{1}{2},n} 1 - \gamma_1}{\xi_{x_{m+\frac{1}{2}}}} + \frac{1}{\xi_{z_n} \Delta z^2} \frac{\eta_{m,n-\frac{1}{2}} 1 - \gamma_2}{\xi_{z_{n-\frac{1}{2}}}} + \rho_{m,n} \omega^2 e, \\ \tilde{d}_4 &= \frac{1}{\xi_{x_m} \Delta x^2} \frac{\mu_{m-\frac{1}{2},n}}{\xi_{x_{m-\frac{1}{2}}}} \gamma_1 - \frac{1}{\xi_{z_n} \Delta z^2} \left(\frac{\eta_{m,n+\frac{1}{2}}}{\xi_{z_{n+\frac{1}{2}}}} + \frac{\eta_{m,n-\frac{1}{2}}}{\xi_{z_{n-\frac{1}{2}}}} \right) \frac{1 - \gamma_2}{2} + \rho_{m,n} \omega^2 d, \\ \tilde{d}_5 &= -\frac{1}{\xi_{x_m} \Delta x^2} \left(\frac{\mu_{m+\frac{1}{2},n}}{\xi_{x_{m+\frac{1}{2}}}} + \frac{\mu_{m-\frac{1}{2},n}}{\xi_{x_{m-\frac{1}{2}}}} \right) \gamma_1 - \frac{1}{\xi_{z_n} \Delta z^2} \left(\frac{\eta_{m,n+\frac{1}{2}}}{\xi_{z_{n+\frac{1}{2}}}} + \frac{\eta_{m,n-\frac{1}{2}}}{\xi_{z_{n-\frac{1}{2}}}} \right) \gamma_2 + \rho_{m,n} \omega^2 c, \\ \tilde{d}_6 &= \frac{1}{\xi_{x_m} \Delta x^2} \frac{\mu_{m+\frac{1}{2},n}}{\xi_{x_{m+\frac{1}{2}}}} \gamma_1 - \frac{1}{\xi_{z_n} \Delta z^2} \left(\frac{\eta_{m,n+\frac{1}{2}}}{\xi_{z_{n+\frac{1}{2}}}} + \frac{\eta_{m,n-\frac{1}{2}}}{\xi_{z_{n-\frac{1}{2}}}} \right) \frac{1 - \gamma_2}{2} + \rho_{m,n} \omega^2 d, \\ \tilde{d}_7 &= \frac{1}{\xi_{x_m} \Delta x^2} \frac{\mu_{m-\frac{1}{2},n} 1 - \gamma_1}{\xi_{x_{m-\frac{1}{2}}}} + \frac{1}{\xi_{z_n} \Delta z^2} \frac{\eta_{m,n+\frac{1}{2}} 1 - \gamma_2}{\xi_{z_{n+\frac{1}{2}}}} + \rho_{m,n} \omega^2 e, \\ \tilde{d}_8 &= -\frac{1}{\xi_{x_m} \Delta x^2} \left(\frac{\mu_{m+\frac{1}{2},n}}{\xi_{x_{m+\frac{1}{2}}}} + \frac{\mu_{m-\frac{1}{2},n}}{\xi_{x_{m-\frac{1}{2}}}} \right) \frac{1 - \gamma_1}{2} + \frac{1}{\xi_{z_n} \Delta z^2} \frac{\eta_{m,n+\frac{1}{2}}}{\xi_{z_{n+\frac{1}{2}}}} \gamma_2 + \rho_{m,n} \omega^2 d, \\ \tilde{d}_9 &= \frac{1}{\xi_{x_m} \Delta x^2} \frac{\mu_{m+\frac{1}{2},n} 1 - \gamma_1}{\xi_{x_{m+\frac{1}{2}}}} + \frac{1}{\xi_{z_n} \Delta z^2} \frac{\eta_{m,n+\frac{1}{2}} 1 - \gamma_2}{\xi_{z_{n+\frac{1}{2}}}} + \rho_{m,n} \omega^2 e, \\ \tilde{c}_1 &= \frac{1}{4\xi_{x_m} \Delta x \Delta z} \frac{\mu_{m-1,n}}{\xi_{z_n}} + \frac{1}{4\xi_{z_n} \Delta x \Delta z} \frac{\lambda_{m,n-1}}{\xi_{x_m}}, \quad \tilde{c}_2 = -\frac{1}{4\xi_{x_m} \Delta x \Delta z} \frac{\mu_{m+1,n}}{\xi_{z_n}} - \frac{1}{4\xi_{z_n} \Delta x \Delta z} \frac{\lambda_{m,n-1}}{\xi_{x_m}}, \\ \tilde{c}_3 &= \frac{1}{4\xi_{x_m} \Delta x \Delta z} \frac{\mu_{m-1,n}}{\xi_{z_n}} - \frac{1}{4\xi_{z_n} \Delta x \Delta z} \frac{\lambda_{m,n+1}}{\xi_{x_m}}, \quad \tilde{c}_4 = \frac{1}{4\xi_{x_m} \Delta x \Delta z} \frac{\mu_{m+1,n}}{\xi_{z_n}} + \frac{1}{4\xi_{z_n} \Delta x \Delta z} \frac{\lambda_{m,n+1}}{\xi_{x_m}}. \end{aligned} \quad (B-9)$$

REFERENCES

- Aki, K., and P. G. Richards, 1980, Quantitative seismology, theory and methods, I: W. H. Freeman and Company.
- Alterman, Z., and F. Karal, 1968, Propagation of elastic waves in layered median by finite differences methods: Bulletin of the Seismological Society of America, **58**, 367–398.
- Cao, J., J. B. Chen, and M. X. Dai, 2016, Improved free-surface expression for frequency-domain elastic optimal mixed-grid modeling: Journal of Applied Geophysics, **130**, 71–80, doi: [10.1016/j.jappgeo.2016.04.010](https://doi.org/10.1016/j.jappgeo.2016.04.010).
- Chen, J.-B., 2012, An average-derivative optimal scheme for frequency-domain scalar wave equation: Geophysics, **77**, no. 6, T201–T210, doi: [10.1190/geo2011-0389.1](https://doi.org/10.1190/geo2011-0389.1).
- Chen, J.-B., 2014, A 27-point scheme for a 3D frequency-domain scalar wave equation based on an average-derivative method: Geophysical Prospecting, **62**, 258–277, doi: [10.1111/1365-2478.12090](https://doi.org/10.1111/1365-2478.12090).
- Gu, B., G. Liang, and Z. Li, 2013, A 21-point finite difference scheme for 2D frequency-domain elastic wave modeling: Exploration Geophysics, **44**, 156–166, doi: [10.1071/EG12064](https://doi.org/10.1071/EG12064).
- House, B., S. Larsen, and J. B. Bednar, 2000, 3-D elastic numerical modeling of a complex salt structure: 70th Annual International Meeting, SEG, Expanded Abstracts, 2201–2204.
- Hustedt, B., S. Operto, and J. Virieux, 2004, Mixed-grid and staggered-grid finite-difference methods for frequency-domain acoustic wave modeling: Geophysical Journal International, **157**, 1269–1296, doi: [10.1111/j.1365-246X.2004.02289.x](https://doi.org/10.1111/j.1365-246X.2004.02289.x).
- Jo, C.-H., C. Shin, and J. H. Suh, 1996, An optimal 9-point, finite-difference, frequency-space, 2-D scalar wave extrapolator: Geophysics, **61**, 529–537, doi: [10.1190/1.1443979](https://doi.org/10.1190/1.1443979).
- Kelly, K. R., S. Treitel, and R. M. Alford, 1976, Synthetic seismograms: A finite difference approach: Geophysics, **41**, 2–27, doi: [10.1190/1.1440605](https://doi.org/10.1190/1.1440605).
- Lysmer, J., and L. A. Drake, 1972, A finite element method for seismology, in B. A. Bolt, ed., Methods in computational physics: Academic Press, Seismology: Surface waves and earth oscillations 11, 181–216.
- Marfurt, K. J., 1984, Accuracy of finite-difference and finite-element modeling of the scalar and elastic wave equations: Geophysics, **49**, 533–549, doi: [10.1190/1.1441689](https://doi.org/10.1190/1.1441689).
- Min, D.-J., C. Shin, B.-D. Kwon, and S. Chung, 2000, Improved frequency-domain elastic wave modeling using weighted-averaging difference operators: Geophysics, **65**, 884–895, doi: [10.1190/1.1444785](https://doi.org/10.1190/1.1444785).
- Mittet, R., 2002, Free-surface boundary conditions for elastic staggered modeling schemes: Geophysics, **67**, 1616–1623, doi: [10.1190/1.1512752](https://doi.org/10.1190/1.1512752).

- Operto, S., J. Virieux, P. Amestoy, J.-Y. L'Excellent, L. Giraud, and H. B. H. Ali, 2007, 3D finite-difference frequency-domain modeling of visco-acoustic wave propagation using a massively parallel direct solver: A feasibility study: *Geophysics*, **72**, no. 5, SM195–SM211, doi: [10.1190/1.2759835](https://doi.org/10.1190/1.2759835).
- Pratt, R. G., 1990, Frequency-domain elastic wave modeling by finite differences: A tool for crosshole seismic imaging: *Geophysics*, **55**, 626–632, doi: [10.1190/1.1442874](https://doi.org/10.1190/1.1442874).
- Pratt, R. G., and M. H. Worthington, 1990, Inverse theory applied to multi-source cross-hole tomography, Part I: Acoustic wave equation method: *Geophysical Prospecting*, **38**, 287–310, doi: [10.1111/j.1365-2478.1990.tb01846.x](https://doi.org/10.1111/j.1365-2478.1990.tb01846.x).
- Shin, C., and H. Sohn, 1998, A frequency-space 2D scalar wave extrapolator using extended 25-point finite-difference operator: *Geophysics*, **63**, 289–296, doi: [10.1190/1.1444323](https://doi.org/10.1190/1.1444323).
- Štekl, I., and R. G. Pratt, 1998, Accurate viscoelastic modeling by frequency-domain finite difference using rotated operators: *Geophysics*, **63**, 1779–1794, doi: [10.1190/1.1444472](https://doi.org/10.1190/1.1444472).
- Xu, Y. X., J. H. Xia, and R. D. Miller, 2007, Numerical investigation of implementation of air-earth boundary by acoustic-elastic boundary approach: *Geophysics*, **72**, no. 5, SM147–SM153, doi: [10.1190/1.2753831](https://doi.org/10.1190/1.2753831).